https://doi.org/10.5194/egusphere-2026-4385
Preprint. Discussion started: 11 August 2026

The impact of Saharan Air Layers on atmospheric stability and clouds during the BOWTIE campaign

Anna Trosits[1,2], Andreas Foth[1], Allison A. Wing[3], Johanna Roschke[1], Moritz Haarig[4], Anton Kötsche[1], and Heike Kalesse-Los[1]

[1]Leipzig Institute for Meteorology, Universität Leipzig, Leipzig, Germany
[2]Institute for Atmospheric and Climate Science, ETH Zurich, Zurich, Switzerland
[3]Department of Earth, Ocean and Atmospheric Science, Florida State University, Tallahassee, FL, USA
[4]Leibniz Institute for Tropospheric Research (TROPOS), Leipzig, Germany

Correspondence: Anna Trosits (anna.trosits@env.ethz.ch) and Heike Kalesse-Los (heike.kalesse-los@uni-leipzig.de)

Abstract.

Clouds over the tropical Atlantic remain under-represented in ground-based observational studies, despite their key role in the regional radiative and hydrological budgets. This observational gap contributes to substantial uncertainties in the representation of these clouds in climate models. The recent BOWTIE (German: Beobachtung von Ozean und Wolken – Das Trans ITCZ Experiment) campaign aimed to address this deficiency through a six-week, ship-borne measurement campaign across the tropical Atlantic, spanning from Cape Verde to Barbados. This study investigates the influence of Saharan Air Layers (SALs) on cloud properties using vertically pointing remote sensing observations collected during the research cruise. Cloud types are classified and combined with Cloudnet-derived microphysical products to assess both macrophysical and microphysical cloud characteristics. The analysis reveals a shift in the cloud characteristics toward less convective regimes during SAL presence, accompanied by changes in cloud base height (CBH) and cloud top height (CTH). Microphysically, the suppression of convection associated with SAL leads to a greater vertical separation of cloud layers, meaning that droplet and ice effective radii (DER and IER) differ across layers. However, hydrometeor populations across all observed layers are comparable to those observed in marine cloud regimes reported in previous studies. Overall, the thermodynamic structure of the SAL emerges as the dominant driver of the observed changes in cloud properties. These findings highlight the importance of accounting for SAL influences in understanding cloud development over the tropical Atlantic and improving their representation in atmospheric models.

1 Introduction

A precise understanding of clouds and the processes driving cloud evolution is crucial for estimating global radiation, energy, and hydrologic balances (e.g. Charlson et al., 1987; Kubar et al., 2009). The energy-rich tropical atmosphere is particularly relevant for estimating the global energy budget due to the high amount of incoming solar radiation, which ultimately drives the global circulation (Kraus, 2007). In general, the impact of clouds on the radiation budget and the hydrological cycle is influenced by cloud macro-properties such as cloud lifetime, depth, base and top height as well as microphysical properties of

https://doi.org/10.5194/egusphere-2026-4385
Preprint. Discussion started: 11 August 2026

hydrometeors such as thermodynamic phase, size, and number concentration (Kubar et al., 2009). These cloud properties are determined by the evolution of the cloud influenced by a variety of processes across a range of scales, which include micro-scale influences such as the presence of aerosols, the diurnal cycle, and meso- to synoptic-scale drivers of moisture availability and atmospheric circulation (Khain et al., 2000; Pan and et al., 2018).

In general, directional and speed convergence at the Intertropical Convergence Zone (ITCZ) are known to govern the formation of convective clouds in the tropics climatologically (Nicholson, 2018; Windmiller and Stevens, 2024). At the synoptic scale, African Easterly Waves (AEW) passing through the tropical Atlantic every three to five days affect deep convection and modulate precipitation formation (Houze and Betts, 1981). Temporally, clouds are influenced by the diurnal cycle of cloud development (Ruppert, 2016). On smaller scales, the presence of aerosols is known to modulate the occurrence of clouds. For aerosol particles over the tropical Atlantic, the dominant source are sea spray from the Atlantic Ocean, biomass burning smoke from the African continent (Barkley et al., 2019) and dust from the Saharan Desert (Guo et al., 2013). An air mass lifted off from the Saharan desert and advected over the Atlantic Ocean contains dust, but also conserves its original thermodynamic properties of temperature and humidity (Gutleben et al., 2019a; Wong and Dessler, 2005). These elevated mixed layers are called Saharan Air Layers (SALs; Tsamalis et al., 2013). The SAL changes its properties due to ageing of the dust aerosols as it travels across the Atlantic (Kanitz et al., 2014; Weinzierl et al., 2017). As previous studies have shown, Saharan dust particles can serve as both, ice nucleating particle (INP) and cloud condensation nuclei (CCN) (DeMott et al., 2003; Twohy et al., 2009; Haarig et al., 2019).

A comprehensive analysis of cloud properties and their evolution requires the synthesis of models and observations to unravel the coupling of various processes and patterns all around the globe (Foltz and McPhaden, 2010; Foltz et al., 2019). It is evident that cloud-related processes are not uniform all over the globe. However, atmospheric observations over ocean regions are under-represented (Foltz et al., 2019) because deployment of instrumentation is difficult and maintenance of instrumentation is negatively impacted by water, salt, erosion and waves. Recent efforts to gain knowledge about clouds over the tropical Atlantic involved modelling and measurements. Field campaigns incorporating comprehensive instrumentation and detailed, targeted observations are a key component of data collection over the tropical ocean, alongside continuous satellite observations and isolated island observing stations, such as the Barbados Cloud Observatory (BCO; Stevens et al., 2016)). Shipborne field campaigns, such as the Global Atmospheric Research Program (GARP) Atlantic Tropical Experiment (GATE) in 1974 (Kuettner, 1974; Kuettner and Parker, 1976) or "ElUcidating the RolE of Cloud–Circulation Coupling in ClimAte" (EUREC^{4}A) in 2020 (Stevens et al., 2021) aimed to investigate clouds, their properties and their link to dynamic patterns over the tropical Atlantic. Previous research cruises from the Caribbean to Cabo Verde were used to study the Saharan dust transport across the Atlantic Ocean (Kanitz et al., 2014; Rittmeister et al., 2017).

In 2024, the "Organized Convection and EarthCARE Studies over the Tropical Atlantic" (ORCESTRA) campaign observed the tropical Atlantic from multiple platforms, investigating the role of mesoscale processes in the context of the climate system (Stevens et al., 2026). As part of ORCESTRA, the sub-campaign "Beobachtung von Ozean und Wolken – Das Trans ITCZ Experiment" (BOWTIE; Translation: ocean and cloud observation - the trans-ITCZ experiment) contained a 40-day-long research cruise across the Atlantic (Klocke et al., 2026). This study, makes use of these shipborne atmospheric observations over

https://doi.org/10.5194/egusphere-2026-4385
Preprint. Discussion started: 11 August 2026

the tropical Atlantic ocean. The proximity of the research cruise to the African continent, and the Saharan Desert, and thus being located in the dust outflow region during the peak season of dust transport (**?**) increases the possibility of atmospheric measurements being influenced by Saharan dust.

The goal of this study is the qualitative description of the influence of SAL on clouds and clouds development during the BOWTIE campaign on a macro- and microphysical scale based on remote sensing and radiosonde observations. Three multi-day periods of Saharan dust were observed by the RV *Meteor* during the campaign. The lidar-based detection of the dust is complemented with other data for the characterisation of the tropospheric conditions and cloud properties during Saharan dust events.

The paper is structured as follows. In Section 2 the data and its processing used for this study is presented. Section 3 describes the methods used for the analysis, including cloud type classification, and the detection and characterisation of SALs. Following a general overview of the cloud conditions in Section 4, the effect of SAL presence on macro- and microphysical properties of clouds is investigated. Finally, a conclusion summarises the derived role of Saharan dust in cloud evolution over the tropical Atlantic in Section 5.

2 Instruments and Data

The observations used in the analysis presented in this paper were gathered as part of the research project ORCESTRA (Stevens et al., 2026) which consisted of eight sub-campaigns including BOWTIE (Klocke et al., 2026).

2.1 The BOWTIE campaign

The BOWTIE sub-campaign, was a ship-borne investigation of atmosphere and ocean onboard the RV *Meteor*, focusing on storm-scale processes, the atmosphere-ocean interaction, and mutual influences (Klocke et al., 2026). The Atlantic crossing started on 16 August west of Africa in Cape Verde and ended in Barbados on 24 September 2024. The westward progression towards Barbados was interrupted by three north-south transects at the beginning, the middle and the end of the campaign period, respectively. The data obtained during BOWTIE is described in more detail by Segura et al. (2026) and is publicly available on the ORCESTRA data browser at: https://browser.orcestra-campaign.org/. BOWTIE collected extensive in situ and remote sensing measurements of atmospheric and oceanic thermodynamic, kinematic, and physical properties. This variety of the instruments allows multiple aspects to be investigated such as the drivers of the large-scale structure of the ITCZ, the variability of convection or small-scale processes at the ocean-atmosphere interface. Remote-sensing and radiosonde data will be used here.

2.2 From instruments to datasets

The instruments used for the investigations presented in this paper are shown in Fig. 1 and mentioned in Tab. 1. The observations were interrupted on 28 August from 8 to 12 UTC while RV *Meteor* was in the territory of Cape Verde. The RPG-HATPRO-G5 Microwave radiometer (MWR; Rose et al., 2005) and the RPG frequency modulated 94 GHz Doppler radar (Küchler et al.,

https://doi.org/10.5194/egusphere-2026-4385
Preprint. Discussion started: 11 August 2026

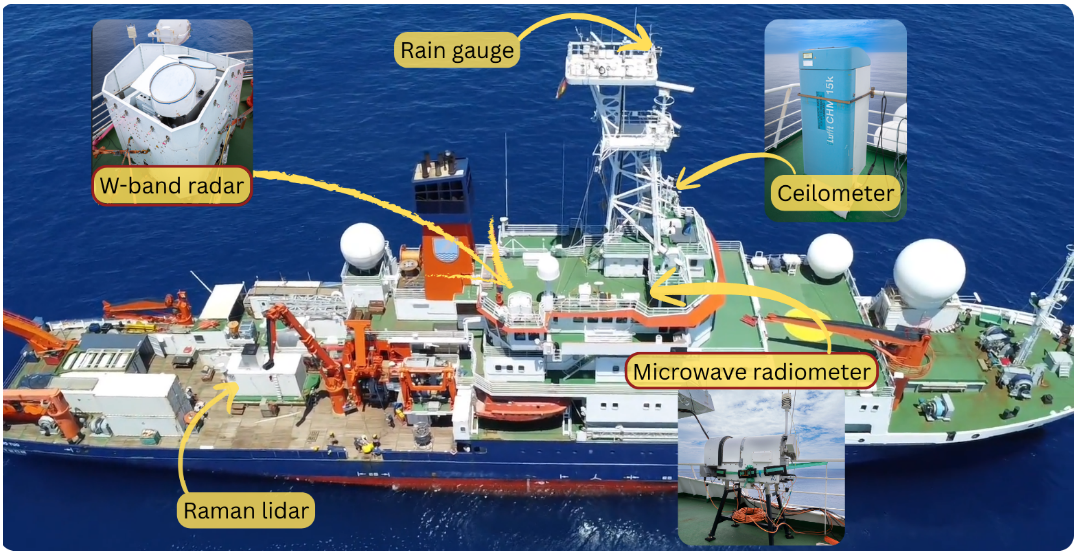

Figure 1. RV *Meteor* during BOWTIE (photo by Geet George (TU Delft)) equipped with remote sensing instruments (photos by Anna Trosits).

Table 1. Specifications of the instrumentation used for the analysis of this paper including information about the operational settings and operators including Leipzig University (LU), the Max Planck Institute for Meteorology (MPI-Met) and the German Weather Service (DWD).

instrument (reference)	wavelength/ frequency	observed quantities	vertical and temporal res.	max. vertical range	operator
Microwave radiometer (Rose et al., 2005)	22.24-31.4 GHz 51-58 GHz	liquid water path	30 s	-	LU
Doppler cloud radar (Küchler et al., 2017)	94 GHz	radar reflectivity factor, Doppler velocity, linear depolarisation ratio	45 m, 1.9 s	9 or 12 km	LU
Ceilometer (Heese et al., 2010)	1064 nm	attenuated backscatter coefficient	15 m, 10 s	15 km	MPI-Met
Raman lidar (MPI-Met)	355, 532 and, 1064 nm	attenuated backscatter coefficient linear depolarisation ratio	60 m, 2 min	29 km	MPI-Met
Radiosondes (Winkler et al., 2026)	-	temperature, relative humidity	10 m	14 km	MPI-Met
Rain gauge (Eigenbrodt GmbH & Co. KG)	-	rain rate	60 s	-	DWD

2017), operated by Leipzig Institute for Meteorology (LIM) were installed on the navigation deck (5th deck) to reduce exposure to sea spray. The MWR sampled atmospheric profiles of temperature and humidity passively with a temporal resolution of 30 s. In addition, every 15 minutes a boundary layer scan was performed. For the MWR, a set of ERA5-based retrievals specifically

https://doi.org/10.5194/egusphere-2026-4385
Preprint. Discussion started: 11 August 2026

for the tropical Atlantic was created as described in Schnitt et al. (2024) using the pyMakeRetrieval routine (Foth, 2023; Foth et al., 2024). The cloud radar was operated in vertical mode and actively detected clouds and precipitation from 150 m to 12 km with a temporal resolution of 1.9 s and a vertical resolution of 15-40 m depending on height.

The operation of a Doppler cloud radar on a ship faces challenges compared to operation on land due to the ship's motion. As the radar was located off centre-point, it experienced vertical (heave) and rotational (pitch, roll, yaw) movement. To counterbalance the misalignment of the radar beam it was deployed in a free swinging cardanic mount as it was during EUREC^{4}A (Kalesse-Los et al., 2023). To correct for the vertical heave in the mean Doppler velocity (MDV) a correction following Acquistapace et al. (2017) was applied, similarly as for the EUREC^{4}A W-band radar data, e.g., presented in Kalesse-Los et al. (2023). Besides the heave correction, the processing chain included the removal of isolated data pixels, Doppler spectrum dealiasing, ghost echo detection and flagging of theses artificial echoes, as well as attenuation due to heavy rain.

Retrievals from the MWR and cloud radar were complemented by data collected by other instruments operated by Max Planck Institute for Meteorology (MPI-Met) and the German Weather Service (DWD). These instruments include a Jenoptik CHM15k ceilometer installed on the 6th deck and the Raman lidar system LICHT (LIdar for Cloud, Humidity and Temperature profiling (MPI-Met) installed on the main deck, in a similar setup as during EUREC^{4}A on the RV *Meteor*. Both instruments were deployed by MPI-Met-Hamburg. The permanently installed rain gauge on the mast of RV *Meteor* was operated by DWD. Specific information about the instruments, the deployment and sampling times can be found in Segura et al. (2026). The ceilometer data is retained in its raw format until it is used in the synergistic Cloudnet algorithm. The Raman lidar data remains uncalibrated, which only allows for a qualitative analysis of the data which is however sufficient for this study. Radiosondes underwent quality control as described in Winkler et al. (2026).

2.3 Limitations of W-band radar observations in the Tropics

Water vapour attenuation of high-frequency radar signals also needs to be considered in the Tropics where high water vapour contents are present (Clothiaux et al., 1995). In the present dataset, W-band radar signal attenuation by water vapour mostly exceeds 5 dB at 5 km altitude (see https://cloudnet.fmi.fi/search/visualizations?site=rv-meteor&dateFrom=2024-08-17&dateTo=2024-08-17&product=categorize&variable=categorize-radar_gas_atten). Additionally, in heavy rain conditions with rain rates exceeding 5 mm/h the observed W-band radar reflectivity at constant altitudes decreased over time even when the rain rate increased. This can be attributed to insufficiently water-repellent radar radomes and/or insufficient rainwater removal by the blowers. Due to its high operating frequency of 94 GHz, the cloud radar signal furthermore cannot penetrate heavy rain (Clothiaux et al., 1995) resulting in a reduced radar echo top height. Thus, the assumption that echo top height corresponds to cloud top height (CTH) does not hold in cases when heavy rain attenuates the radar signal. In the analysis of CTH, this would distort the results and is, therefore, flagged and left out for the respective analysis of CTHs.

2.4 Cloudnet products

The European research project Cloudnet started in 2002 to optimize the representation of clouds in forecast models. From a combination of ground-based remote-sensing instruments, standardized NetCDF datasets (https://cloudnet.fmi.fi) are created

https://doi.org/10.5194/egusphere-2026-4385
Preprint. Discussion started: 11 August 2026

for evaluation across stations (Illingworth et al., 2007). Processing is performed by the CloudnetPy package (Tukiainen et al., 2020), using Doppler cloud radar, ceilometer, microwave radiometer, and rain gauge data, combined with thermodynamic profiles from models or radiosondes. After interpolation to 30 m and 30 s resolution, each pixel is classified for hydrometeors, cloud phase, aerosols, or insects (Hogan and O'Connor, 2004). A pixel represents the smallest unit of measurement in both time and space within the Cloudnet dataset. From the categorization, drizzle, liquid, and ice pixels are identified. The interested reader is referred to the original paper by Hogan and O'Connor (2004) for additional information about the Cloudnet target classification procedure.

For pixels identified as liquid containing, Droplet Effective Radius (DER) is derived based on radar reflectivity following the method of Frisch et al. (2002). The liquid-water content (LWC) is derived by constraining adiabatic profiles with MWR-based LWP over the vertical extent of the cloud (Illingworth et al., 2007). For pixels identified as ice containing, ice water content (IWC) can be derived based on radar reflectivity and model temperature (Hogan et al., 2006). The IWC retrieval relying on the Rayleigh assumption was developed for midlatitude stratiform ice clouds, so its global use, especially for observations in the Tropics, is uncertain. Moreover, at 94 GHz, the Rayleigh assumption becomes invalid for large ice crystals, with additional errors resulting from attenuation by liquid water and melting ice (Hogan et al., 2006). Cloudnet derives Ice Effective Radius (IER) from IWC and lidar extinction (Delanoë et al., 2007) using the reflectivity–temperature relationship of Griesche et al. (2020). IWC and extinction errors at 94 GHz can be large (Hogan et al., 2006; Tukiainen et al., 2025), generally exceeding those at 35 GHz and increasing with decreasing temperature (Hogan et al., 2006). A summary of uncertainties of Cloudnet retrieved microphysical products can be found in Tukiainen et al. (2025). While uncertainties increase when applying these relationships outside their original data range, these retrievals are nevertheless critically needed (e.g., as microphysical input to radiative transfer simulations to estimate cloud radiative effects), particularly beyond midlatitudes.

Acknowledging these uncertainties, we nonetheless show results for the Tropics, relying on Cloudnet's quality flags to limit errors in the statistics of the microphysical products. The Cloudnet internal retrieval status for its microphysical products, provides eight different quality status classifications among which only "feasible" and "retrieval performed with radar corrected for liquid, melting or melting attenuation" are used in this study.

3 Methodology

In order to obtain more general results when assessing the influence of SAL on clouds, the clouds are classified according to their macrophysical properties. In addition, the actual period of the occurrence of Saharan dust must be determined as an indicator of SAL. The properties of the dust layer are then related to those of a SAL.

3.1 Cloud type classification

A cloud type classification facilitates the characterisation of occurrence of clouds in different height ranges. A threshold-based classification using macrophysical properties such as cloud base and top height was applied. An echo mask of W-band radar reflectivity is used, considering all pixels with valid reflectivities. The object-based approach based on Roschke et al. (2025)

https://doi.org/10.5194/egusphere-2026-4385
Preprint. Discussion started: 11 August 2026

identifies connected pixels in the cloud mask as one object and subsequently derives metrics for that object; for example, the index (or here, height) of lower and upper edge and the area in pixel units. The criteria for the metrics per cloud type class are chosen in agreement with typical climatological cloud classes, following previous studies (Schulz et al., 2021). Johnson et al. (1999) pointed out that there are three major modes of convective cloud types in the tropics. Following this, convective clouds most frequently occur as cumulus humilis (CuHum), cumulus congestus (CuCon), and cumulonimbus (Cb). These three types all have a cloud base height (CBH) at the lifting condensation level (LCL) and are only differentiated by their vertical extension in the form of CTH (Table A1). However, observations indicate that not all clouds align with these aforementioned categories. We thus include two additional classes. The alto cloud class, identified by a CBH above the LCL and the cloud top below or only slightly above the 0 °C-isotherm, contains alto cumulus and alto stratus in the mid-levels of the troposphere. The high cloud class includes isolated cirrus or mixed-phase clouds with bases above the 0 °C-isotherm. In addition to these clearly defined clouds, convective clouds may also be coincidentally connected to another stratus cloud or may produce outflow (Schulz et al., 2021). These connected clouds were added to the CuCon class because the characteristics of the few connected cloud cases were very similar to CuCon. While other cloud types could be distinguished (such as a separation of warm and mixed-phase alto clouds), for simplicity we restrict our analysis to five classes: CuHum, CuCon, Cb, Alto, and High clouds (Figure 2).

This classification has several limitations. The object-based analysis of radar data can lead to pixels being connected incorrectly. For example, the seeder-feeder effect of higher clouds precipitating into lower clouds is not separated here, because there uncertainty and misclassification remains even with separating these two cloud layers with connected pixels. However, a visual inspection of the misclassified clouds revealed that incorrect classifications are rare.

3.2 Saharan dust detection

Within the dataset of the BOWTIE campaign, three periods of Saharan dust occurrence were identified based on Raman lidar observations. Specifically, mineral dust presence was identified by enhanced Particle Linear Depolarisation Ratio (PLDR) in combination with near-zero backscatter-related Ångström exponent (Floutsi et al., 2023). The enhanced PLDR results from the non-sphericity of fresh and aged dust aerosol particles, which distinguishes them from, e.g., marine or pollution aerosol particles that can also occur over the open ocean (Bohlmann et al., 2018). The three Saharan dust periods observed above the RV *Meteor* are highlighted in orange in the bottom bar of Fig. 4. In each case, the Saharan dust remained in the troposphere for several days. It should be noted that the Raman lidar system LICHT remained uncalibrated, meaning that the depolarisation ratio cannot be used quantitatively derive the amount of dust. Still, microphysical properties can be identified qualitatively (personal communication with instrument-operator Ilya Serikov), and therefore, can be used for dust aerosol identification. Enhanced depolarisation ratios indicate mineral dust layers with typical values of the PLDR of 0.25 to 0.35 (Haarig et al., 2017; Veselovskii et al., 2016). The uncalibrated PLDRs indeed show an enhancement in depolarisation ratio in the SAL compared to the marine aerosol layer below, but the values are quantitatively too low because of the missing calibration. The dusty periods were verified by satellite observations and model forecasts.

https://doi.org/10.5194/egusphere-2026-4385
Preprint. Discussion started: 11 August 2026

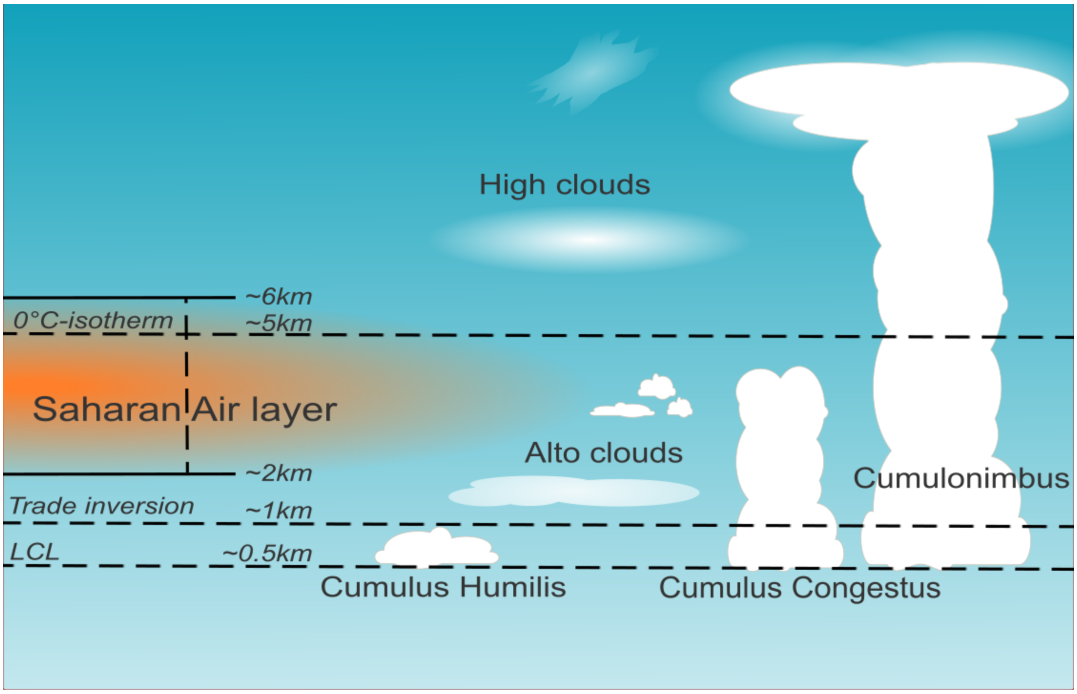

Figure 2. Visualisation of applied cloud type scheme.

190 Specifically, the Geostationary Operational Environmental Satellite (GOES) 16 providing the Split Window product for SAL detection (Dunion and Velden, 2004; Dunion, 2011), is visualised in Fig. 3B, A1B and A2B (retrieved from: University of Wisconsin - CIMSS at https://tropic.ssec.wisc.edu/archive/index.php?basin=EuropeAfrica&searchmethod=date&startdate=20240825&enddate=20240928&ptimes=00,03,06,09,12,15,18,21). The algorithm of the Split Window product is sensitive to the presence of dry and/or dusty air in the lower to middle levels of the atmosphere (600-925 hPa or 4,500-800 m) and is 195 denoted by yellow to pink shading (Dunion and Velden, 2004). The pink-white shading qualitatively indicates likely SAL regions with increased amount of dust content and dry lower-tropospheric air. These SAL layers were present in the GOES16 observations during the identified dust event periods from the shipborne data, though the dust layer is not clearly present in the satellite images at all times due to the presence of clouds. However, the Copernicus Atmosphere Monitoring Service (CAMS) Dust aerosol optical depth at 550 nm forecast indicates the three periods of Saharan dust presence (data retrieved 200 from: (Copernicus Atmosphere Monitoring Service, 2021)) thus further validating the ship-based SAL identification.

The strongest of the three dust periods was observed above the ship from 28 August until 31 August 2024, when the RV *Meteor* was located at approximately 25 °W (see panel B in Fig. 3). This dust period (referred to as Saharan dust case 3) is presented in detail in Fig. 3, which provides an overview of the CAMS AOD, GOES 16 Split-Window product as well as Raman lidar, cloud radar, and radiosonde observations. A similar overview of the two other dust periods can be found in the appendix 205 (Figs. A1 and A2). During the strongest dusty period, the dust layer was first observed on 28 August, 3 UTC at a height of 5 km as a very thin layer. Over time, the vertical extent expanded downward at the same time the PLDR intensified, as can be seen

https://doi.org/10.5194/egusphere-2026-4385
Preprint. Discussion started: 11 August 2026

Fig. 3E. The top of the layer was consistently observed at around 5 km, while the base lowered from 5 km at 6 UTC to 2.5 km at 24 UTC on 28 August. The dust layer persisted stably until 30 August, 4 UTC with CuCon clouds directly below the dust layer during 29 August. This gives the impression of the clouds being capped by the dust layer, which will be discussed in the next subsection. On 30 August at around 6 UTC, clouds occurred at the top and above the dust layer precipitating into lower tropospheric layers. These were classified as Alto clouds and produced virga, which led to wet deposition and reduced the height and load of the dust layer. The dust layer eventually faded out on 31 August at 3 UTC. Apart from the dust plume in an altitude of 2.5 – 5 km, an aerosol layer in the lowest 2 km exhibiting strong backscatter and lower depolarisation compared to the dust plume with Ångström exponent values less than one was observed from 28 August to 29 August 6 UTC. This suggests that the source was marine aerosol particles (Bohlmann et al., 2018). In the following, the Saharan dust periods are defined as times when dust occurred, regardless of its height.

3.3 Saharan air layer identification and characterisation

The lower the ambient temperature, the more active are dust INP for immersion nucleation (Kanji et al., 2019). In warm clouds, the hygroscopicity of Saharan dust can lead to an increased number of cloud droplets with smaller radii (Rosenfeld et al., 2001; Twohy et al., 2009) which in turn leads to precipitation suppression during dust events. Ageing and shape-induced differential fallout of dust particles (Yang et al., 2013), leads to a change in the characteristics of SAL during its transport across the Atlantic Ocean (Groß et al., 2015; Gasteiger et al., 2017; Weinzierl et al., 2017). Of the three observed dust cases, only the third case represents a well-mixed dust layer at an altitude of two to five kilometres with a vertical structure as described by Barreto et al. (2022) (see Fig. 3). The first dust case (24 August to 27 August) shows signatures of the shape-related differential sedimentation of spherical dust particles by the gradual decrease of PLDR towards the ground (see Fig. A1) (Yang et al., 2013). Saharan dust is advected within an air layer which is also thermodynamically characterised by its dry, well mixed origin over the Saharan desert (Tsamalis et al., 2013; Barreto et al., 2022). For the identification of SAL, Saharan dust is a sufficient tracer (Tsamalis et al., 2013) and can be detected by considering several Raman lidar variables (e.g., Gebauer et al., 2026). The detection of dust and with it SAL identification was described before. In the following the characteristics of the air layer, in which the dust is suspended are analysed.

In addition to the vertically pointing remote-sensing observations by lidar and radar (panels C–E and F, respectively), the profiles of relative humidity and lapse rate derived from radiosondes are shown in panels G and H of Fig. 3. The height of the dust layer derived from PLDR is visualised by grey shading in panels F to H. These dust-laden layers coincide with observations of lower relative humidities of around 40 % by the radiosondes. The lapse rate profiles also exhibit signatures of an air mass origin different than oceanic regions: While the moisture-rich atmosphere above the tropical Atlantic theoretically exhibits a moist-adiabatic temperature gradient (–0.6 K/100 m), the temperature gradient in the dust layer is more negative than in the marine environment and approaches a dry-adiabatic lapse rate of around –1 K/100 m as shown in panel H of Fig. A3 and Fig. 3. The dry-adiabatic lapse rate is an indicator of the air mass' origin over the arid, continental Saharan desert. Due to the lack of moisture and strong diurnal adiabatic heating, the air mass over the Saharan desert exhibits a strongly mixed atmospheric

https://doi.org/10.5194/egusphere-2026-4385
Preprint. Discussion started: 11 August 2026

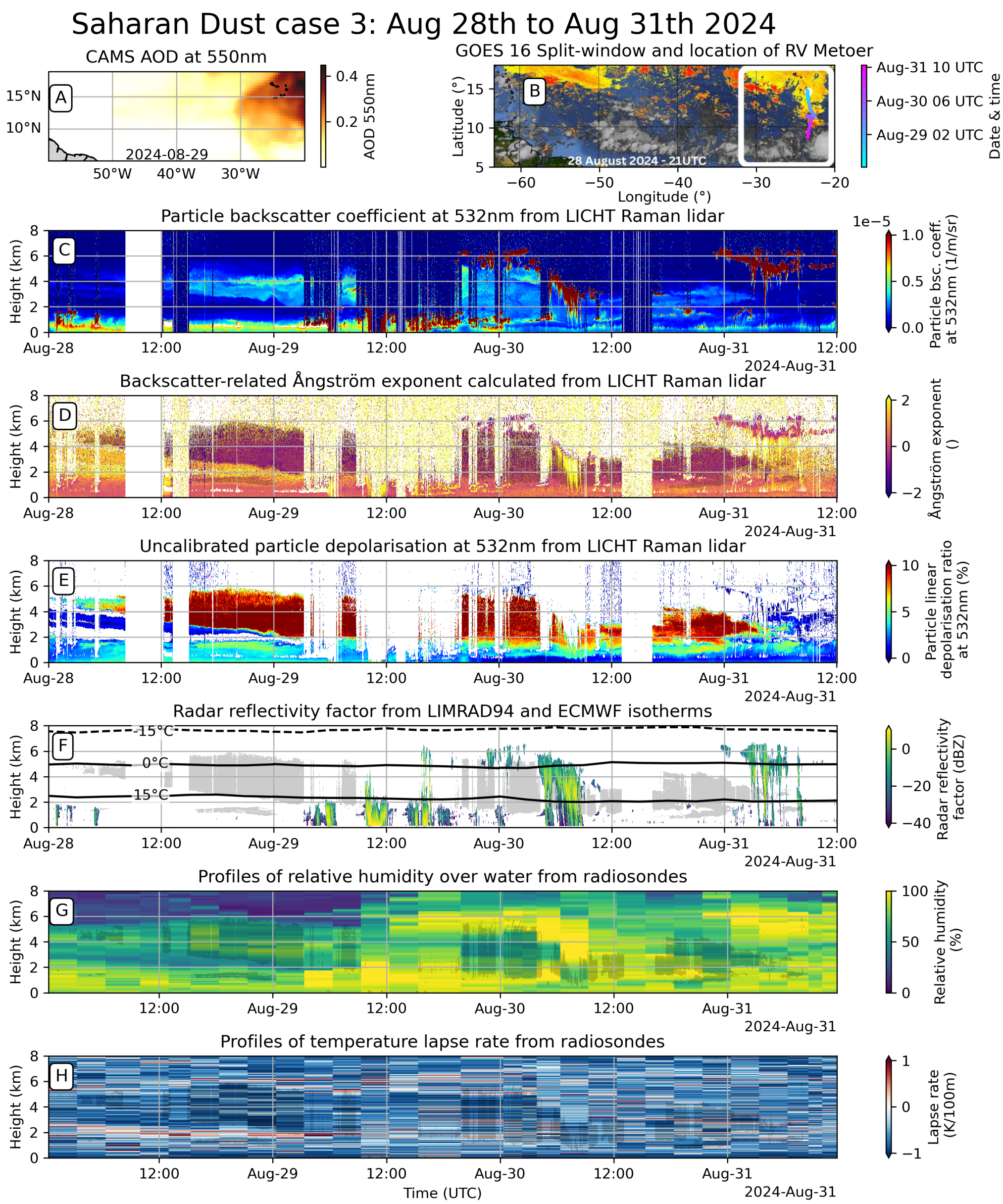

Figure 3. Saharan dust case 3 - Overview including the CAMS aerosol optical depth at 550 nm (A), location of RV *Meteor* and image of SAL split-window product of GOES16 (B), Raman lidar particle backscatter coefficient at 532 nm (C), lidar backscatter related Ångström exponent (D), uncalibrated PLDR (E), LIMRAD94 cloud radar reflectivity and ECMWF isotherms (F), profiles of relative humidity over water and lapse rate profiles from radiosonde observations (G and H), respectively. Panels F, G and H contain a grey shading for areas with PLDR$> 5\,\%$.

https://doi.org/10.5194/egusphere-2026-4385
Preprint. Discussion started: 11 August 2026

boundary layer with a great vertical extent, which leads to a near dry adiabatic lapse rate up to 4 – 5 km above ground (Tesche et al., 2009).

Additionally, at the bottom and top of the dust layer temperature inversions are evident in the radiosonde data. As also reported in the literature, the lower edge inversion results from the lifting and advection of the dry and hot continental air mass over cooler airmass over the ocean (Barreto et al., 2022). The upper boundary temperature inversion develops due to the comparatively strong temperature decrease with height of the continental air mass, resulting in a lower temperature at the top of the dust-rich air layer compared to the air above it. The vertical structure of such an advected, well-mixed elevated dust layer between two and five kilometres was also described by Yang et al. (2013), Weinzierl et al. (2017) and Barreto et al. (2022) and is characteristic of the Saharan Air Layer (Tsamalis et al., 2013).

Here, the three observed SAL cases are characterised by drier air inside the layer (around 50 %in case 3, Fig. 3), at the lower SAL edge (around 20 % in case 2, Fig. A2) or at the upper SAL edge (around 30 % in case 1, Fig. A1). However, as e.g. evident in Fig. 3 G, the relative humidity in the lower part of SAL is higher than in the upper half. Consequently, bounding inversions are conserved and enhanced heating rates occur at the ocean's surface (Gutleben et al., 2019b). This in turn leads to lower tropospheric stabilisation and mid-level tropospheric destabilisation (Wong and Dessler, 2005; Barreto et al., 2022). The following section evaluates the effect of the three detected SALs on the observed cloud properties.

4 Results: The effect of Saharan air layers on clouds during BOWTIE

The effect of Saharan dust and the surrounding SAL on the atmosphere during BOWTIE is assessed by an investigation at several scales. The general cloud occurrence introduced in Fig. 4 illustrates the variability of cloudiness and rainfall throughout the campaign. The following sections analyse the influence of the presence of Saharan dust on the macro- and microphysical characteristics of clouds, such as CBH and CTH, cloud depth and hydrometeor effective radii. To assure comparability between the different data subsets, the "no Saharan dust" period was limited to times when the RV *Meteor* was operating in approximately the same geographical region where Saharan dust was observed. This condition was met until 2 September, when the vessel began its east–west transect toward Barbados and crossed 27° W. As a result, the dataset comprises 8.2 days with dust and 7.8 days without dust. These intervals are considered the most comparable in terms of environmental conditions and are hereafter referred to as the "Saharan Dust" and "No Saharan Dust" periods.

4.1 Clouds during BOWTIE

Figure 4 provides a first insight into the cloudiness during BOWTIE, based on the number of hours per day of clear-sky, cloudy, and rainy conditions. The rain flag was derived from the rain gauge measurements. The "confidently cloudy" and "probably cloudy" cloudy classes result from signals received by either the ceilometer or cloud radar ("probably cloudy"), or both ("confidently cloudy") following Schnitt et al. (2024). The class "probably cloudy" mostly occurred when the ceilometer detected a thin layer of mid-level cloud at around 4 km altitude. These clouds often remained undetected by the cloud radar due to strong water vapour attenuation of up to 4 dB at 4 km altitude.

https://doi.org/10.5194/egusphere-2026-4385
Preprint. Discussion started: 11 August 2026

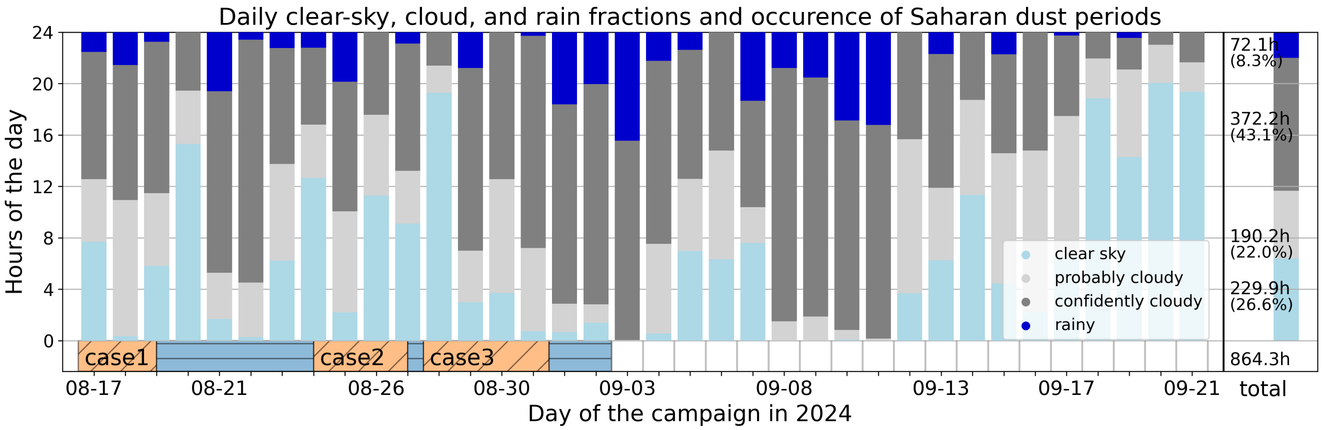

Figure 4. Ambient conditions as hours per day of cloud and rain occurrence, with classes “clear sky”, “probably cloudy”, “confidently cloudy” and “rainy” based on radar, ceilometer and rain gauge signals. Orange indicates the cases of Saharan dust. The blue shading indicates the periods of dust free conditions in the same region as the observed dust, therefore serving as comparison period.

As shown in Fig. 4, there was a high day-to-day variability in cloud and rainfall occurrence above RV *Meteor* in the first third of the campaign (to 27°W). From 30 August until 11 September, the troposphere was cloudier and it rained more frequently. This period was followed by many days with clear skies and little rain from 12 September until the end of the campaign when the ship steamed west of 35°W en route to Barbados. This demonstrates that the cloud cover and rainfall are strongly variable across the tropical Atlantic. A similar pattern of cloudiness and precipitation occurrence was revealed by observations with Sea-Pol, a scanning C-band radar (Rutledge et al., 2019; Klocke et al., 2026).Multiple factors affect cloudiness, such as environmental humidity (Schulz and Stevens, 2018), for example. Moreover, the synoptic-scale influence of troughs and ridges associated with African easterly waves modulates the occurrence of cloud clusters (Houze and Betts, 1981) and precipitation (Janiga and Thorncroft, 2016). A diurnal cycle in cloud evolution driven by radiative processes could be expected (Ruppert, 2016) but was not evident in the surface precipitation dataset of the rain gauge likely because of the limited temporal and spatial extent of this vertically pointing 40-day long dataset (not shown). Another variable that influences cloud occurrence is the presence of an advected SAL from the African continent, which contains suspended Saharan desert dust (Weinzierl et al., 2017). Due to natural variability of atmospheric processes, multiple influences on cloud characteristics need to be taken into in account for a comprehensive cloud development study, which limits the results of this study.

4.2 Cloud type distributions

As described in section 3.3, the thermodynamic structure of the SAL, in which the Saharan dust is suspended, increases the stability of the lower troposphere through temperature inversions at the bottom and top of the SAL, as well as through net heating of the lower troposphere at the ocean surface. Weak convection either cannot overcome the energy barrier at the inversion or it dries out by entrainment in the lowest part of the SAL (Wong and Dessler, 2005; Yang et al., 2013; Gutleben

https://doi.org/10.5194/egusphere-2026-4385
Preprint. Discussion started: 11 August 2026

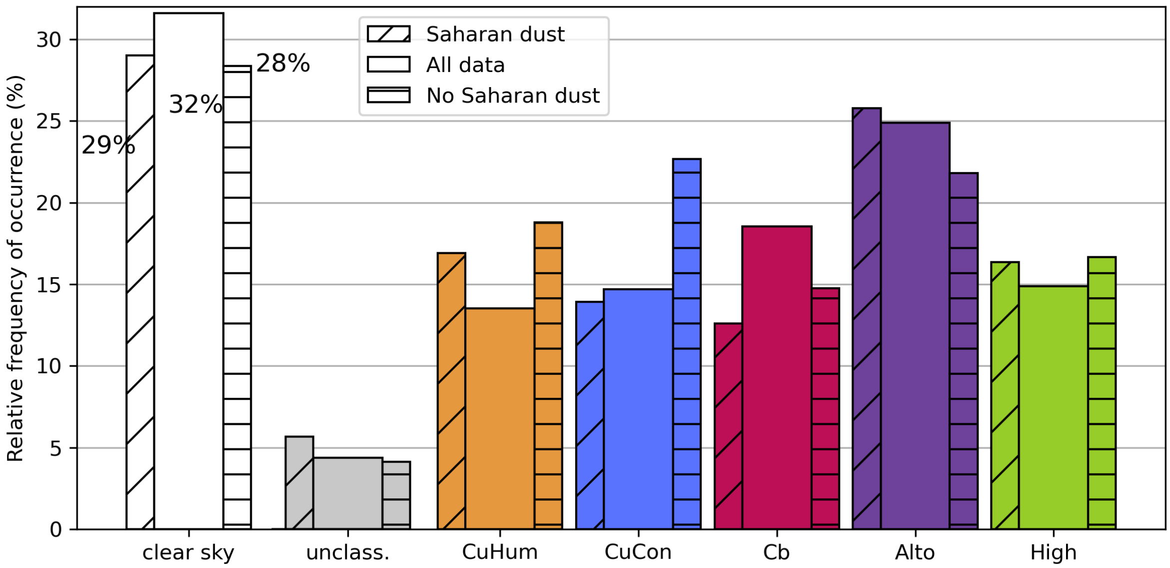

Figure 5. Relative temporal frequency of occurrence of different cloud types for the all data of the whole campaign (17.Aug 2024 - 22.Sep) and the sub-periods in the Eastern Atlantic with (17.Aug 00 UTC -19.Aug 12 UTC, 24.Aug 22 UTC - 27.Aug 4 UTC and 28.Aug 00 UTC - 31.Aug 12 UTC) and without (19.Aug 12 UTC - 24.Aug 22 UTC, 27.Aug 4 UTC - 28.Aug 00 UTC, 31.Aug 12 UTC - 2 Sep 2024 00 UTC) Saharan dust .

et al., 2019b). Meanwhile, the stability of the mid level troposphere is decreased due to stronger lapse rates. Presumably, once a larger, cold-pool driven meso-scale convective system (MCS) grows beyond the temperature inversion, it could profit from the increased lapse rates. However, in the given dataset, this situation was not observed.

Fig. 5 shows how this affects the distribution of cloud types by contrasting periods with and without dust present in the same region. A Jensens-Shannon test showed that the overall distributions of cloud type are similar but distinguishable. The differences are more notable between the dusty and non-dusty periods (JS = 0.08) than when comparing the period of Saharan dust to all data, which also contains the dusty sub-periods (JS = 0.07). Bootstrap resampling reveals, that the differences in the distributions of cloud types of dusty to non-dusty conditions are statistically driven by differences in the occurrence of CuCon and alto clouds. At the same time the difference between dusty periods and all data is mainly caused by differences in Cb occurrence. A lower frequency of convective clouds classes (CuHum, CuCon and Cb) during Saharan dust periods suggests a reduction of convection. In particular, the frequency of CuCon clouds decreases in the presence of Saharan dust by about one third compared to when no dust was observed, which is in agreement with Wong and Dessler (2005) and Gutleben et al. (2019a). However, the decrease in CuHum frequency is only minor and suggests that they are not affected by the SAL but are rather formed in the convective boundary layer from sea salt aerosols. Additionally, alto clouds were found to occur more frequently when dust was observed (Fig. 5, Fig. 3). Meanwhile, high clouds remain mostly unaffected by the SAL and their frequency remains similar.

https://doi.org/10.5194/egusphere-2026-4385
Preprint. Discussion started: 11 August 2026

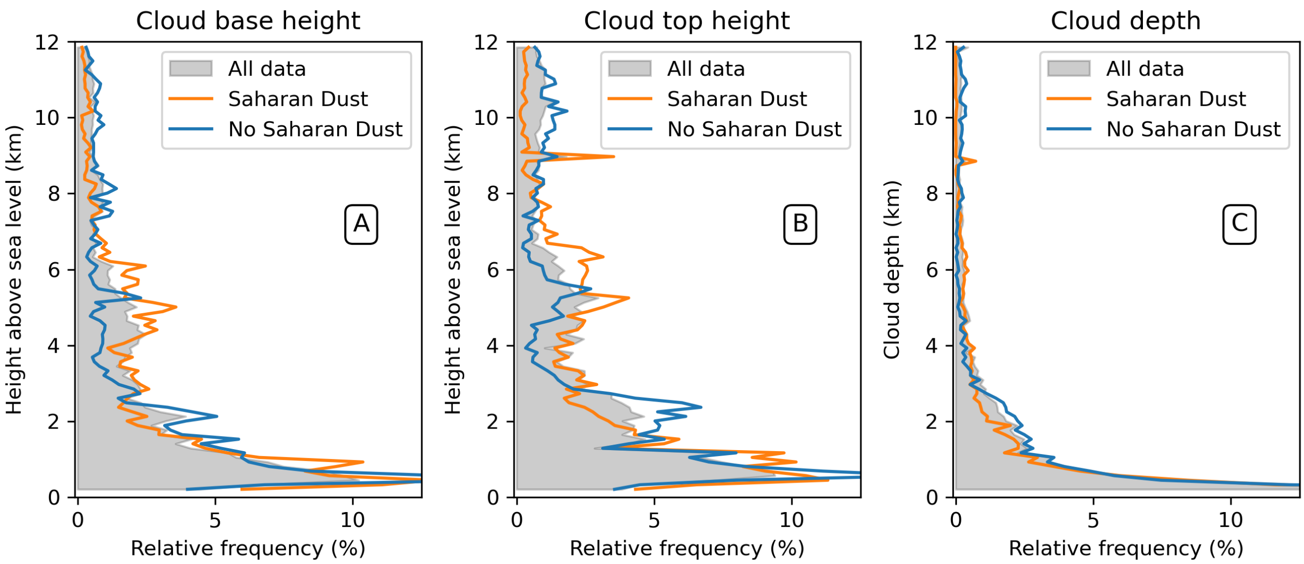

Figure 6. Distribution of cloud top height, cloud base height and cloud depth for Saharan dust times and the non-dusty periods.

4.3 Macrophysical cloud properties

Fig. 6 presents the distribution of CBH and CTH, as well as the cloud depth, at a vertical resolution of 120 m. The data are shown for the whole campaign period, as well as separately for dusty and non-dusty periods in the eastern tropical Atlantic. Due to quality and accuracy constraints induced data gaps, the lowest two cloud radar height ranges (below 150 m) are excluded. Additionally, cloud depths of two pixels (with a height of 30 m per pixel) or less are neglected. Due to multi-layer cloud occurrences, the accumulated relative frequencies of all CBH, CTH and depth, in relation to the time during which clouds were present, can exceed 100 %. A major limitation of the cloud radar-derived CBH and CTH distribution is the cloud radar signal attenuation by high IWV, which increases with height and makes thin, liquid alto clouds undetectable for the radar.

The enhanced occurrence of alto clouds (Fig. 5) is also evident in the distribution of CBH and CTH. CBHs and CTH in the altitude of the upper boundary of the SAL (4–7 km, see schematic in Fig. 2) are more frequent in the presence of Saharan dust. Moreover, in the periods of no Saharan dust, cloud bases and tops occur more frequently at altitudes below 3 km and above 8 km. Lower CTHs aligned with previous studies (e.g. Gutleben et al., 2019a; Wong and Dessler, 2005), which have found that shallow marine trade wind clouds exhibit reduced CTHs, cloud fraction and horizontal cloud extend as a macrophysical effect of a SAL in the troposphere. For high clouds, the visual ratio of CBH to CTH in SAL-free conditions is also indicative for the presence of more cirrus clouds and more Cbs with cloud tops extending beyond 9 km. This is also evident in cloud depth distributions. However, the cloud depth distribution clearly peaks at low vertical extents, indicating the ubiquitous presence of thin cloud layers in both SAL and SAL-free conditions. The enhanced occurrence of alto clouds in dusty periods only occurs at the top of the SAL in approximately 6 km altitude. However, from this analysis, the expected role of dust as CCN

https://doi.org/10.5194/egusphere-2026-4385
Preprint. Discussion started: 11 August 2026

or INP can not be evaluated. Instead, the increased atmospheric stability rather suppresses the formation of convection, as it was also observed by (e.g. Wong and Dessler, 2005; Barreto et al., 2022). Ultimately, this case reveals that the SAL's moisture and temperature characteristics dominate over any expected CCN-driven cloud enhancement by dust particles in the BOWTIE dataset. Nevertheless, the role of dust particles as INPs is not negligible: alto clouds occurred more frequently at the top of the SAL than in its absence, suggesting a potential link to dust-induced ice formation.

4.4 Microphysical cloud properties

The Cloudnet-derived variables DER, IER, LWC, and IWC provide microphysical insights into cloud processes, which are eventually relevant for the cloud radiative effect. The distributions of the aforementioned quantities are studied for dusty and non-dusty periods and for individual cloud types. The distributions for DER and IER are shown in Fig. 7, panels A and B, respectively. As no significant differences in LWC and IWC were found between the SAL and non-SAL periods they are not shown here. The distributions of DER for the three considered time periods (Saharan dust, no Saharan dust and all data) have the same width, peaking at 8 µm. The modality of the distributions exhibits differences between the dusty and non-dusty observation periods. During Saharan dust cases, the DER distributions can be described as a bimodal distribution consisting of two droplet populations. One population with effective droplet sizes between 5 and 10 µm originates from CuHum, CuCon, Cb and Alto clouds (see Fig. 7 panel C). Smallest DER were found for CuHum, followed by DER of CuCon. The small secondary peak of larger droplets of around 22 µm effective radius results from Cb and Alto clouds, probably in mixed-phase regions. Tolentino et al. (2026) observed an increase in DER in single-layer mixed-phase clouds compared to purely liquid clouds, but the radii did not grow beyond 15 µm. The considered single-layer mixed-phase clouds differ from the DER in convective clouds containing both, liquid and ice. In mixed-phase alto clouds the difference can also result from precipitation or retrieval uncertainties, since it mostly occurred for the retrieval status "radar corrected for attenuation". Generally, DER in the mixed-phase regime was found to be larger than for pure liquid-clouds.

Panel C and E in Fig. 7 show the contribution of the different cloud types to the total DER distribution. Since the SAL and non-SAL periods exhibit a different distribution of cloud types, the DER distribution is also expected to differ. Here, the CuCon clouds have a range of DER with only one peak at 8 µm. Depending on the selected period, the distribution of CuCon dominates the total DER distribution and makes the different droplet populations indistinguishable. This behaviour is observed in liquid-containing clouds during the non-dusty period.

The IER distribution in Fig. 7 B shows a feature similar to the DER bimodal size distribution in 7 A. Even though ice particle growth mechanisms are different from the processes responsible for droplet growth, isolated cloud layers, as observed in dusty periods, lead to a bimodal IER distribution. The two distinguishable IER size distributions are especially prevalent in high clouds (see Fig. 7 panel D). However, all three distributions peak at around 50 µm and have near-identical width. The peak in the number of small ice crystals during periods of Saharan dust (IER around 32 µm) is caused by very high, isolated cirrus clouds that are not anvil-related as e.g. from 29 to 31 August, 2024. Comparing the IER distribution to Griesche et al. (2020), shows that the high clouds in non dusty conditions follow a very similar shape and values of the distribution. However, the total distributions of IER are also affected by Cb and Alto clouds related ice detection and IER calculations.

https://doi.org/10.5194/egusphere-2026-4385
Preprint. Discussion started: 11 August 2026

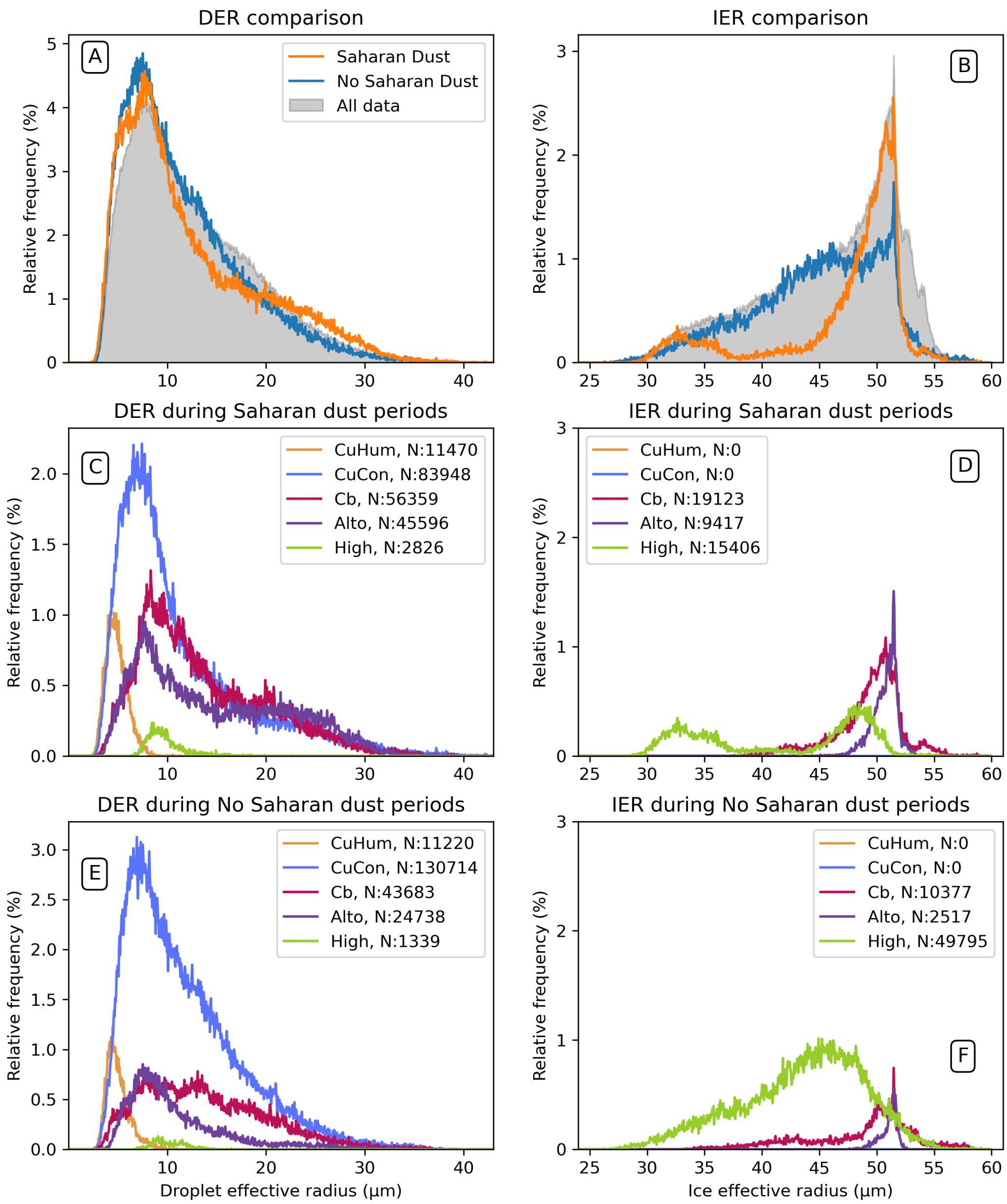

Figure 7. Distribution of DER and IER for Saharan dust times and the non-dusty periods and the entire dataset.

360

https://doi.org/10.5194/egusphere-2026-4385
Preprint. Discussion started: 11 August 2026

5 Conclusions

In this work, we derived cloud statistics for the BOWTIE field campaign and investigate the effect of the SAL on the atmosphere and cloud macro- and microphysical properties. For this purpose, we exploited a unique ship-based remote sensing dataset obtained during a transect across the tropical Atlantic ITCZ. The comprehensive set of high-resolution measurements enabled the application of the Cloudnet processing chain, including data quality control and cloud retrievals, and provided continuous observations of clouds in the tropical ITCZ over extended periods. In this way, key limitations of previous aircraft- and satellite-based studies, which were restricted by either short sampling periods or coarser spatial and temporal resolution, were overcome. The dataset is publicly available and provides a valuable benchmark for satellite evaluation and model-observation studies.

In the case studies (Fig. 3 and Fig. A1), we observed that the SAL suppression of convection associated with the moisture and temperature characteristics of air masses originating from the African continent. The dry desert air, exhibiting dry adiabatic conditions within the SAL, bounded by inversions at its bottom and top, inhibit cloud vertical development. Weak convection is capped by the SAL base, because the energy barrier for further ascend is increased (Wong and Dessler, 2005). These findings suggest that the thermodynamic properties of SAL dominate over potential hygroscopic effects of the mineral dust acting as CCN, consistent with Gutleben et al. (2019a). The resulting suppression of convection modifies the cloud type distribution (Fig. 5), reducing the number of deep convective clouds while increasing the number of Alto clouds. Furthermore, cloud layers become more distinctly separated during SAL conditions owing to reduced convective mixing leading to bimodal distributions of IER and DER (Fig. 7). Although Alto clouds occur more frequently near the SAL top , the the available observations do not allow us to disentangle microphysical effects of dust acting as INPs from the thermodynamic effects of the SAL.

Overall, our results demonstrate that the SAL influences cloud macro- and microphysical properties, including suppression of convection, enhanced cloud-layer separation, and emergence of bimodal DER and IER distributions, primarily through its stabilising effect on the lower troposphere. While the strongly negative lapse rate within the dry SAL can increase mid-tropospheric instability, this appears to play a minor role for weak convection because entrainment of the dry air suppresses the development of individual convective cells. These changes in cloud structure are likely associated with modifications in cloud radiative properties and lifetime and thus may influence the surface energy budget. However, direct assessment of these impacts was beyond the scope of our observational setup, which does not permit tracking clouds throughout their life cycle. In addition, uncertainties inherent to remote-sensing retrievals must be considered when interpreting the derived cloud properties. More case studies and even long-term measurements are therefore required to assess the robustness and representativeness of the observed SAL effects. Long-term measurements at SAL influenced sites equipped with comparable instrumentation, such as Mindelo (Cape Verde) or Ragged Point (Barbados), would provide appropriate basis for such investigations. Nevertheless, by providing a unique, openly available Cloudnet-processed dataset from the tropical Atlantic ITCZ and new observational evidence of SAL-cloud interactions, this study establishes an important foundation for future process studies, model evaluation, and improved representation of aerosol-cloud interactions in weather and climate models.

https://doi.org/10.5194/egusphere-2026-4385
Preprint. Discussion started: 11 August 2026

Data availability. The data used here, is publicly available on the ORCESTRA data browser, under the following links:

Cloudnet (LIMRAD94 cloud radar, microwave radiometer and derived cloud macro- and microphysical products):

https://doi.org/10.82246/bafybeidtfyua2vmmrpnhbl6nj57x2ynowaceghdapyetc6lnrpjii2tlli

Rain gauge: https://doi.org/10.82246/bafybeievu3hvrmcb7bh6fv4xqsx3kzsreokwknsk2mfz62xp2fspyzrrta

Ceilometer: https://doi.org/10.82246/bafybeia74wnxe2nxwkcmespzjckqwt25tyhcknah3xqxxeeevbsdiawzom

Microwave Radiometer (HATPRO - single point): https://doi.org/10.82246/bafybeihc63mpkfatnvl6z5hze2eijzwqr6o3ohubhi5i66dvos4qjcssvu

Microwave Radiometer (HATPRO - multiple point): https://doi.org/10.82246/bafybeihddiylirtiv64yo74wzt7zok545yowhiiu23kjonvz2wl57eunze

Raman lidar licht (fast product - 2 min smoothing): https://doi.org/10.82246/bafybeidhokylvrnu447th4z3npevzflfmtjsva2icf7gbyp7mmsyyeknhm

Raman lidar licht (slow product - 58 min smoothing): https://doi.org/10.82246/bafybeie754xlrs75yw2vnqrneuh23vsalzagfputvjnbqnsi4fvyjjtfrq

Appendix A

A1

https://doi.org/10.5194/egusphere-2026-4385
Preprint. Discussion started: 11 August 2026

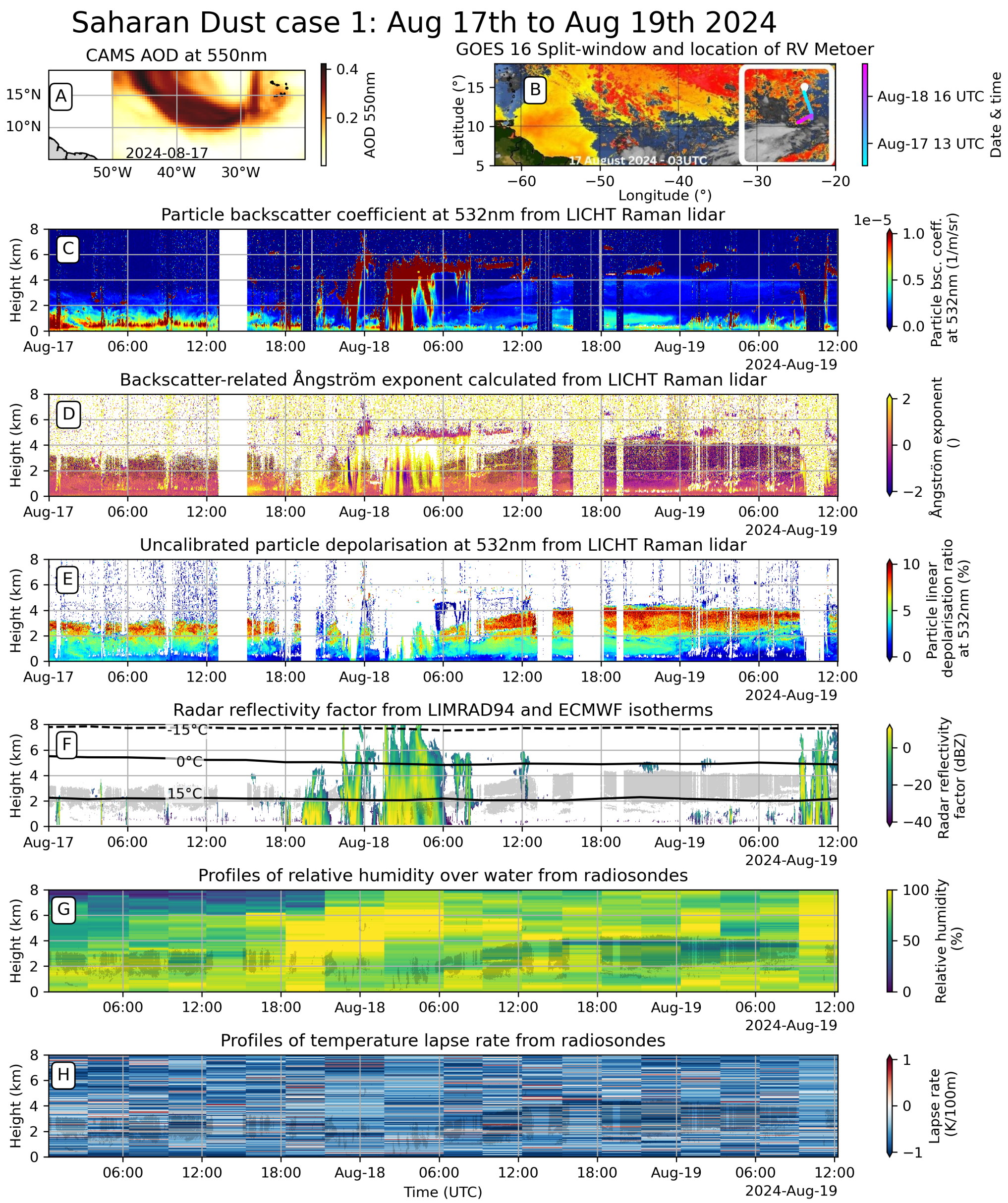

Figure A1. Saharan dust case 1 - Overview including the CAMS aerosol optical depth at 550 nm (A), the location of RV *Meteor* and the image of SAL split-window product of GOES16 (B), particle backscatter coefficient at 532 nm (C), the backscatter related Ångström exponent (D), uncalibrated PLDR (E), radar reflectivity (F), relative humidity profiles and lapse rate profiles from radiosonde observations (G and H) respectively. Panels F, G and H contain a grey shading for areas with PLDR$>5\,\%$.

https://doi.org/10.5194/egusphere-2026-4385
Preprint. Discussion started: 11 August 2026

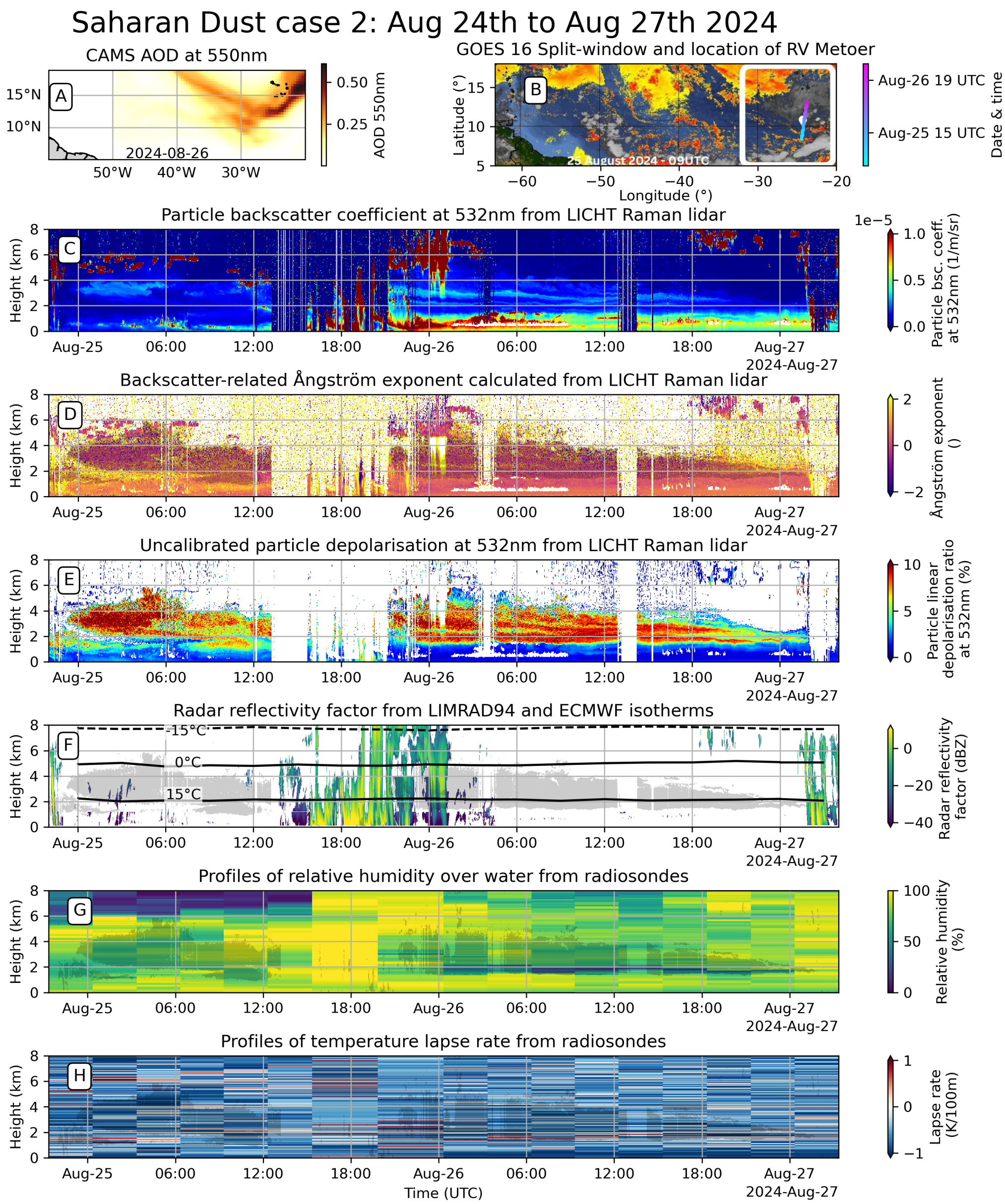

Figure A2. Saharan dust case 2 - Overview including the CAMS aerosol optical depth at 550 nm (A), the location of RV *Meteor* and the image of SAL split-window product of GOES16 (B), particle backscatter coefficient at 532 nm (C), the backscatter related Ångström exponent (D), uncalibrated PLDR (E), radar reflectivity (F), relative humidity profiles and lapse rate profiles from radiosonde observations (G and H) respectively. Panels F, G and H contain a grey shading for areas with PLDR$>5\,\%$.

https://doi.org/10.5194/egusphere-2026-4385
Preprint. Discussion started: 11 August 2026

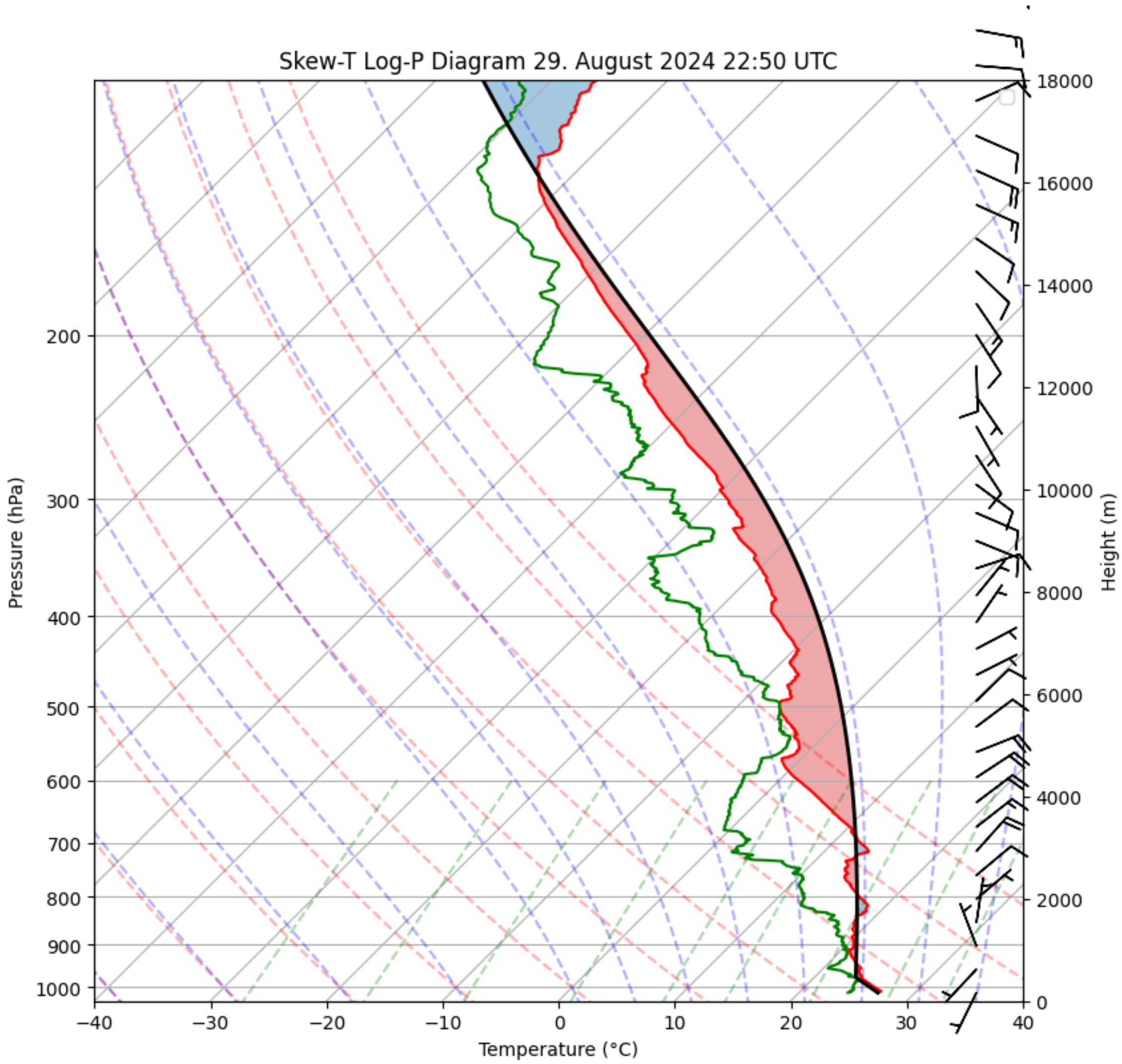

Figure A3. SkewT diagramm of 29. August 2024 launched from RV Meteor at 22:50 UTC

https://doi.org/10.5194/egusphere-2026-4385
Preprint. Discussion started: 11 August 2026

Table A1. Cloud classification thresholds, grey labels = flexible threshold,

Type	short name	Object base	object top
High clouds	High	above 0 °C-isotherm	above 0 °C-isotherm
Alto clouds	Alto	above LCL	below 0 °C-isotherm
Cumulus Humilis	CuHum	below LCL	below 1 km
Cumulus Congestus	CuCon	below LCL	below 0 °C-isotherm
Cumulonimbus	Cb	below LCL	-

Author contributions. AT collected and analysed data, created the figures, conceptualised and wrote the draft of the paper. HK-L supervised the analysis and the development of the concept of the paper. AF and AK prepared data, shared their expertise in discussions and contributed to the manuscript. MH and AAW provided input and knowledge for the analysis and contributed to the manuscript. JR provided the basis of the cloud type classification and contributed to the manuscript.

Competing interests. The authors declare that they have no conflict of interest.

Disclaimer. This study is based on the master thesis from which some parts are not substantially modified.

Acknowledgements. We acknowledge ACTRIS and Finnish Meteorological Institute for processing our data with the Cloudnet processing chain and for making our dataset available for download from https://cloudnet.fmi.fi. The authors acknowledge Jonas Witthuhn, Moritz Lochmann, and Johannes Röttenbacher who helped installing the LU instrumentation on RV Meteor, and Robert Mackenzie and the crew of RV *Meteor* cruise M203 for the support of operating and dismantling the LU instrumentation during the research campaign. Thanks go to Ilya Serikov for the discussions on the LICHT lidar data set. Declaration of AI use: In this study, artificial intelligence was used for the following purposes: DeepL and Copilot were used to the improvement of language style of texts. ChatGPT, perplexity.ai and Copilot assisted in the development of code for plotting routines and statistical metrics. Research Rabbit and perplexity.ai supported the literature research by finding relevant literature.

Financial Support. The funding for the BOWTIE campaign and the RV *Meteor* cruise M203 was provided by the Deutsche Forschungsgemeinschaft (DFG) under grant number GPF20-1 072. We gratefully acknowledge the funding by the DFG – project no. 268020496 – TRR 172, within the Transregional Collaborative Research Center “ArctiC Amplification: Climate Relevant Atmospheric and SurfaCe Processes, and Feedback Mechanisms (AC)3 for the work of AF. AAW is supported by NSF AGS through Award No. 2331199. This work by JR was funded by the Leibniz ScienceCampus ‘Smoke and bioaerosols in a changing climate’ (BioSmoke) and supported by the Leibniz competition (project number W86/2023). This contribution by AK was funded by the Deutsche Forschungsgemeinschaft (DFG, German Research Foundation) – Project number: 408008112

https://doi.org/10.5194/egusphere-2026-4385
Preprint. Discussion started: 11 August 2026

(Characterization of orography-influenced riming and secondary ice production and their effects on precipitation rates using radar polarimetry and Doppler spectra – CORSIPP) within the Priority Program SPP 2115 “Polarimetric Radar Observations meet Atmospheric Modelling (PROM) – Fusion of Radar Polarimetry and Numerical Atmospheric Modelling Towards an Improved Understanding of Cloud and Precipitation Processes. ORCESTRA was made possible thanks to the support of the Max Planck Society (MPG), the European Research Council through Grant No. 101098063, the Deutsche Forschungsgemeinschaft (DFG, German Research Foundation), the German Aerospace Center (DLR), the German Federal Ministry for Education and Research (BMBF), the French National Centre for Scientific Research (CNRS), the Dutch Research Council (NWO), the European Space Agency (ESA), and the US National Science Foundation (NSF).

https://doi.org/10.5194/egusphere-2026-4385
Preprint. Discussion started: 11 August 2026

References

Acquistapace, C., Kneifel, S., Löhnert, U., Kollias, P., Maahn, M., and Bauer-Pfundstein, M.: Optimizing observations of drizzle onset with millimeter-wavelength radars, Atmospheric Measurement Techniques, 10, 1783–1802, https://doi.org/10.5194/amt-10-1783-2017, 2017.

Barkley, A. E., Prospero, J. M., Mahowald, N., Hamilton, D. S., Popendorf, K. J., Oehlert, A. M., Pourmand, A., Gatineau, A., Panechou-Pulcherie, K., Blackwelder, P., and Gaston, C. J.: African biomass burning is a substantial source of phosphorus deposition to the Amazon, Tropical Atlantic Ocean, and Southern Ocean, Proceedings of the National Academy of Sciences, 116, 16 216–16 221, https://doi.org/10.1073/pnas.1906091116, 2019.

Barreto, , Cuevas, E., García, R. D., Carrillo, J., Prospero, J. M., Ilić, L., Basart, S., Berjón, A. J., Marrero, C. L., Hernández, Y., and Bustos, J. J.: Long-term characterisation of the vertical structure of the Saharan Air Layer over the Canary Islands using lidar and radiosonde profiles: implications for radiative and cloud processes over the subtropical Atlantic Ocean, Atmospheric Chemistry and Physics, 22, 739–763, https://doi.org/https://doi.org/10.5194/acp-22-739-2022, 2022.

Bohlmann, S., Baars, H., Radenz, M., Engelmann, R., and Macke, A.: Ship-borne aerosol profiling with lidar over the Atlantic Ocean: from pure marine conditions to complex dust–smoke mixtures, Atmospheric Chemistry and Physics, 18, 9661–9679, https://doi.org/10.5194/acp-18-9661-2018, 2018.

Charlson, R. J., Lovelock, J. E., Andreae, M. O., and Warren, S. G.: Oceanic phytoplankton, atmospheric sulphur, cloud albedo and climate, Nature, 326, 655–661, https://doi.org/10.1038/326655a0, 1987.

Clothiaux, E. E., Miller, M. A., Albrecht, B. A., Ackerman, T. P., Verlinde, J., Babb, D. M., Peters, R. M., and Syrett, W. J.: An Evaluation of a 94-GHz Radar for Remote Sensing of Cloud Properties, Journal of Atmospheric and Oceanic Technology, 12, 201–229, https://doi.org/10.1175/1520-0426(1995)012<0201:aeoagr>2.0.co;2, 1995.

Copernicus Atmosphere Monitoring Service: CAMS global atmospheric composition forecasts, https://doi.org/10.24381/04a0b097, accessed on 12.02.2026, 2021.

Delanoë, J., Protat, A., Bouniol, D., Heymsfield, A., Bansemer, A., and Brown, P.: The characterization of ice cloud properties from Doppler radar measurements, Journal of Applied Meteorology and Climatology, 46, 1682–1698, https://doi.org/https://doi.org/10.1175/JAM2543.1, 2007.

DeMott, P. J., Sassen, K., Poellot, M. R., Baumgardner, D., Rogers, D. C., Brooks, S. D., Prenni, A. J., and Kreidenweis, S. M.: African dust aerosols as atmospheric ice nuclei, Geophysical Research Letters, 30, https://doi.org/10.1029/2003gl017410, 2003.

Dunion, J. P.: Rewriting the Climatology of the Tropical North Atlantic and Caribbean Sea Atmosphere, Journal of Climate, 24, 893–908, https://doi.org/10.1175/2010jcli3496.1, 2011.

Dunion, J. P. and Velden, C. S.: The Impact of the Saharan Air Layer on Atlantic Tropical Cyclone Activity, Bulletin of the American Meteorological Society, 85, 353–366, https://doi.org/10.1175/bams-85-3-353, 2004.

Eigenbrodt GmbH & Co. KG: Ship Rain Gauge SRM 450, https://www.eigenbrodt.de/en/products/meteorologie/ship-rain-gauge-srm-450/, https://www.eigenbrodt.de/en/products/meteorologie/ship-rain-gauge-srm-450/, accessed on 14.06.2026.

Floutsi, A. A., Baars, H., Engelmann, R., Althausen, D., Ansmann, A., Bohlmann, S., Heese, B., Hofer, J., Kanitz, T., Haarig, M., Ohneiser, K., Radenz, M., Seifert, P., Skupin, A., Yin, Z., Abdullaev, S. F., Komppula, M., Filioglou, M., Giannakaki, E., Stachlewska, I. S., Janicka, L., Bortoli, D., Marinou, E., Amiridis, V., Gialitaki, A., Mamouri, R.-E., Barja, B., and Wandinger, U.: DeLiAn – a growing collection of depolarization ratio, lidar ratio and Ångström exponent for different aerosol types and mixtures from ground-based lidar observations, Atmospheric Measurement Techniques, 16, 2353–2379, https://doi.org/10.5194/amt-16-2353-2023, 2023.

https://doi.org/10.5194/egusphere-2026-4385
Preprint. Discussion started: 11 August 2026

Foltz, G. R. and McPhaden, M. J.: Interaction between the Atlantic meridional and Niño modes, Geophysical Research Letters, 37, https://doi.org/10.1029/2010gl044001, 2010.

Foltz, G. R., Brandt, P., Richter, I., Rodríguez-Fonseca, B., Hernandez, F., Dengler, M., Rodrigues, R. R., Schmidt, J. O., Yu, L., Lefevre, N., Da Cunha, L. C., McPhaden, M. J., Araujo, M., Karstensen, J., Hahn, J., Martín-Rey, M., Patricola-DiRosario, C. M., Poli, P., Zuidema, P., Hummels, R., Perez, R. C., Hatje, V., Lübbecke, J. F., Polo, I., Lumpkin, R., Bourlès, B., Asuquo, F. E., Lehodey, P., Conchon, A., Chang, P., Dandin, P., Schmid, C., Sutton, A., Giordani, H., Xue, Y., Illig, S., Losada, T., Grodsky, S. A., Gasparin, F., Lee, T., Mohino, E., Nobre, P., Wanninkhof, R., Keenlyside, N., Garcon, V., Sánchez-Gómez, E., Nnamchi, H. C., Drévillon, M., Storto, A., Remy, E., Lazar, A., Speich, S., Goes, M., Dorrington, T., Johns, W. E., Moum, J. N., Robinson, C., Perruche, C., de Souza, R. B., Gaye, A. T., López-Parages, J., Monerie, P.-A., Castellanos, P., Benson, N. U., Hounkonnou, M. N., Duhá, J. T., Laxenaire, R., and Reul, N.: The Tropical Atlantic Observing System, Frontiers in Marine Science, 6, https://doi.org/10.3389/fmars.2019.00206, 2019.

Foth, A.: remsens-lim/pyMakeRetrieval: pyMakeRetrieval v1.1.1, https://doi.org/10.5281/ZENODO.10014291, 2023.

Foth, A., Lochmann, M., Saavedra Garfias, P., and Kalesse-Los, H.: Determination of low-level temperature profiles from microwave radiometer observations during rain, Atmospheric Measurement Techniques, 17, 7169–7181, https://doi.org/10.5194/amt-17-7169-2024, 2024.

Frisch, S., Shupe, M., Djalalova, I., Feingold, G., and Poellot, M.: The Retrieval of Stratus Cloud Droplet Effective Radius with Cloud Radars, Journal of Atmospheric and Oceanic Technology, 19, 835–842, https://doi.org/10.1175/1520-0426(2002)019<0835:troscd>2.0.co;2, 2002.

Gasteiger, J., Groß, S., Sauer, D., Haarig, M., Ansmann, A., and Weinzierl, B.: Particle settling and vertical mixing in the Saharan Air Layer as seen from an integrated model, lidar, and in situ perspective, Atmospheric Chemistry and Physics, 17, 297–311, https://doi.org/10.5194/acp-17-297-2017, 2017.

Gebauer, H., Floutsi, A. A., Hofer, J., Haarig, M., Skupin, A., Engelmann, R., Jimenez, C., Wagner, R., and Baars, H.: Characterization of the annual cycle of atmospheric aerosol over Mindelo, Cabo Verde, by means of continuous multiwavelength lidar observations, Atmospheric Chemistry and Physics, 26, 3439–3465, https://doi.org/10.5194/acp-26-3439-2026, 2026.

Griesche, H. J., Seifert, P., Ansmann, A., Baars, H., Barrientos Velasco, C., Bühl, J., Engelmann, R., Radenz, M., Zhenping, Y., and Macke, A.: Application of the shipborne remote sensing supersite OCEANET for profiling of Arctic aerosols and clouds during <i>Polarstern</i> cruise PS106, Atmospheric Measurement Techniques, 13, 5335–5358, https://doi.org/10.5194/amt-13-5335-2020, 2020.

Groß, S., Freudenthaler, V., Schepanski, K., Toledano, C., Schäfler, A., Ansmann, A., and Weinzierl, B.: Optical properties of long-range transported Saharan dust over Barbados as measured by dual-wavelength depolarization Raman lidar measurements, Atmospheric Chemistry and Physics, 15, 11 067–11 080, https://doi.org/10.5194/acp-15-11067-2015, 2015.

Guo, Y., Tian, B., Kahn, R. A., Kalashnikova, O., Wong, S., and Waliser, D. E.: Tropical Atlantic dust and smoke aerosol variations related to the Madden-Julian Oscillation in MODIS and MISR observations, Journal of Geophysical Research: Atmospheres, 118, 4947–4963, https://doi.org/10.1002/jgrd.50409, 2013.

Gutleben, M., Groß, S., and Wirth, M.: Cloud macro-physical properties in Saharan-dust-laden and dust-free North Atlantic trade wind regimes: a lidar case study, Atmospheric Chemistry and Physics, 19, 10 659–10 673, https://doi.org/10.5194/acp-19-10659-2019, 2019a.

Gutleben, M., Groß, S., Wirth, M., Emde, C., and Mayer, B.: Impacts of Water Vapor on Saharan Air Layer Radiative Heating, Geophysical Research Letters, 46, 14 854–14 862, https://doi.org/10.1029/2019gl085344, 2019b.

Haarig, M., Ansmann, A., Althausen, D., Klepel, A., Groß, S., Freudenthaler, V., Toledano, C., Mamouri, R.-E., Farrell, D. A., Prescod, D. A., Marinou, E., Burton, S. P., Gasteiger, J., Engelmann, R., and Baars, H.: Triple-wavelength depolarization-ratio profiling

https://doi.org/10.5194/egusphere-2026-4385
Preprint. Discussion started: 11 August 2026

of Saharan dust over Barbados during SALTRACE in 2013 and 2014, Atmospheric Chemistry and Physics, 17, 10 767–10 794, https://doi.org/10.5194/acp-17-10767-2017, 2017.

Haarig, M., Walser, A., Ansmann, A., Dollner, M., Althausen, D., Sauer, D., Farrell, D., and Weinzierl, B.: Profiles of cloud condensation nuclei, dust mass concentration, and ice-nucleating-particle-relevant aerosol properties in the Saharan Air Layer over Barbados from polarization lidar and airborne in situ measurements, Atmospheric Chemistry and Physics, 19, 13 773–13 788, https://doi.org/10.5194/acp-19-13773-2019, 2019.

Heese, B., Flentje, H., Althausen, D., Ansmann, A., and Frey, S.: Ceilometer lidar comparison: backscatter coefficient retrieval and signal-to-noise ratio determination, Atmospheric Measurement Techniques, 3, 1763–1770, https://doi.org/10.5194/amt-3-1763-2010, 2010.

Hogan, R. J. and O'Connor, E. J.: Facilitating cloud radar and lidar algorithms: the Cloudnet Instrument Synergy/Target Categorization product, Cloudnet documentation, 14, 2004.

Hogan, R. J., Mittermaier, M. P., and Illingworth, A. J.: The Retrieval of Ice Water Content from Radar Reflectivity Factor and Temperature and Its Use in Evaluating a Mesoscale Model, Journal of Applied Meteorology and Climatology, 45, 301–317, https://doi.org/10.1175/jam2340.1, 2006.

Houze, R. A. and Betts, A. K.: Convection in GATE, Reviews of Geophysics, 19, 541–576, https://doi.org/10.1029/RG019i004p00541, 1981.

Illingworth, A. J., Hogan, R. J., O'Connor, E., Bouniol, D., Brooks, M. E., Delanoé, J., Donovan, D. P., Eastment, J. D., Gaussiat, N., Goddard, J. W. F., Haeffelin, M., Baltink, H. K., Krasnov, O. A., Pelon, J., Piriou, J.-M., Protat, A., Russchenberg, H. W. J., Seifert, A., Tompkins, A. M., van Zadelhoff, G.-J., Vinit, F., Willén, U., Wilson, D. R., and Wrench, C. L.: Cloudnet, Bulletin of the American Meteorological Society, 88, 883–898, https://doi.org/10.1175/BAMS-88-6-883, 2007.

Janiga, M. A. and Thorncroft, C. D.: The Influence of African Easterly Waves on Convection over Tropical Africa and the East Atlantic, Monthly Weather Review, 144, 171–192, https://doi.org/10.1175/MWR-D-14-00419.1, 2016.

Johnson, R. H., Rickenbach, T. M., Rutledge, S. A., Ciesielski, P. E., and Schubert, W. H.: Trimodal Characteristics of Tropical Convection, Journal of Climate, 12, 2397–2418, https://doi.org/10.1175/1520-0442(1999)012<2397:TCOTC>2.0.CO;2, 1999.

Kalesse-Los, H., Kötsche, A., Foth, A., Röttenbacher, J., Vogl, T., and Witthuhn, J.: The Virga-Sniffer – a new tool to identify precipitation evaporation using ground-based remote-sensing observations, Atmospheric Measurement Techniques, 16, 1683–1704, https://doi.org/10.5194/amt-16-1683-2023, 2023.

Kanitz, T., Engelmann, R., Heinold, B., Baars, H., Skupin, A., and Ansmann, A.: Tracking the Saharan Air Layer with shipborne lidar across the tropical Atlantic, Geophysical Research Letters, 41, 1044–1050, https://doi.org/10.1002/2013GL058780, 2014.

Kanji, Z. A., Sullivan, R. C., Niemand, M., DeMott, P. J., Prenni, A. J., Chou, C., Saathoff, H., and Möhler, O.: Heterogeneous ice nucleation properties of natural desert dust particles coated with a surrogate of secondary organic aerosol, Atmospheric Chemistry and Physics, 19, 5091–5110, https://doi.org/https://doi.org/10.5194/acp-19-5091-2019, 2019.

Khain, A., Ovtchinnikov, M., Pinsky, M., Pokrovsky, A., and Krugliak, H.: Notes on the state-of-the-art numerical modeling of cloud microphysics, Atmospheric Research, 55, 159–224, https://doi.org/10.1016/S0169-8095(00)00064-8, 2000.

Klocke, D., Wing, A. A., Segura, H., Dengler, M., Bell, M. M., Ruppert, J. H., George, G., Kalesse-Los, H., Nuijens, L., Möller, K. O., Kiko, R., Mohr, W., Kidane, A. T., Trosits, A., Mertz, C., Imker, C., Begler, C., Blandfort, D., Colón-Burgos, D., Austen, D., Junyent, F., Schmidt, H., Habib, J., van der Giessen, J., Wieners, K.-H., Hayo, L., Stelzner, M., Lovato, M., O'Driscoll, O., Paschou, P., Henning, P., Mackenzie, R., Wimmer, W., Serikov, I., Brügmann, B., Wu, Y., Stevens, B., and Windmiller, J.: 40 Days and Nights in the Rains: The Inner Life of the Atlantic ITCZ during BOWTIE, Bulletin of the American Meteorological Society, 107, E1656–E1672, https://doi.org/10.1175/bams-d-25-0166.1, 2026.

https://doi.org/10.5194/egusphere-2026-4385
Preprint. Discussion started: 11 August 2026

Kraus, H.: Die Atmosphäre der Erde, Springer Berlin Heidelberg, Berlin, Heidelberg, 3 edn., ISBN 978-3-540-20656-9, https://doi.org/10.1007/3-540-35017-9, 2007.

Kubar, T. L., Hartmann, D. L., and Wood, R.: Understanding the Importance of Microphysics and Macrophysics for Warm Rain in Marine Low Clouds. Part I: Satellite Observations, Journal of the Atmospheric Sciences, 66, 2953–2972, https://doi.org/10.1175/2009JAS3071.1, 2009.

Küchler, N., Kneifel, S., Löhnert, U., Kollias, P., Czekala, H., and Rose, T.: A W-Band Radar–Radiometer System for Accurate and Continuous Monitoring of Clouds and Precipitation, Journal of Atmospheric and Oceanic Technology, 34, 2375–2392, https://doi.org/10.1175/jtech-d-17-0019.1, 2017.

Kuettner, J. P.: General description and central program of GATE, Bulletin of the American Meteorological Society, 55, 712–719, http://www.jstor.org/stable/26255635, 1974.

Kuettner, J. P. and Parker, D. E.: GATE: Report on the field phase, sciences, 57, 11–27, 1976.

MPI-Met: LICHT Raman Lidar System at the Barbados Cloud Observatory, https://wiki.mpimet.mpg.de/doku.php?id=observations:bco:ramanlidars:raman-lidar-licht, accessed 14 June 2026.

Nicholson, S. E.: The ITCZ and the Seasonal Cycle over Equatorial Africa, Bulletin of the American Meteorological Society, 99, 337–348, https://doi.org/10.1175/BAMS-D-16-0287.1, 2018.

Pan, B. and et al.: Impacts of Saharan Dust on Atlantic Regional Climate and Implications for Tropical Cyclones, Journal of Climate, 31, 7621–7644, https://doi.org/10.1175/jcli-d-16-0776.1, 2018.

Rittmeister, F., Ansmann, A., Engelmann, R., Skupin, A., Baars, H., Kanitz, T., and Kinne, S.: Profiling of Saharan dust from the Caribbean to western Africa – Part 1: Layering structures and optical properties from shipborne polarization/Raman lidar observations, Atmospheric Chemistry and Physics, 17, 12 963–12 983, https://doi.org/10.5194/acp-17-12963-2017, 2017.

Roschke, J., Witthuhn, J., Klingebiel, M., Haarig, M., Foth, A., Kötsche, A., and Kalesse-Los, H.: Discriminating between “drizzle or rain” and sea salt aerosols in Cloudnet for measurements over the Barbados Cloud Observatory, Atmospheric Measurement Techniques, 18, 487–508, https://doi.org/10.5194/amt-18-487-2025, 2025.

Rose, T., Crewell, S., Löhnert, U., and Simmer, C.: A network suitable microwave radiometer for operational monitoring of the cloudy atmosphere, Atmospheric Research, 75, 183–200, https://doi.org/10.1016/j.atmosres.2004.12.005, 2005.

Rosenfeld, D., Ridich, Y., and Lahav, R.: Desert dust suppressing precipitation: A possible desertification feedback loop, Proceedings of the National Academy of Sciences of the USA, 98, 5975–5980, https://doi.org/https://doi.org/10.1073/pnas.101122798, 2001.

Ruppert, J. H.: Diurnal timescale feedbacks in the tropical cumulus regime, Journal of Advances in Modeling Earth Systems, 8, 1483–1500, https://doi.org/10.1002/2016MS000713, 2016.

Rutledge, S. A., Chandrasekar, V., Fuchs, B., George, J., Junyent, F., Dolan, B., Kennedy, P. C., and Drushka, K.: SEA-POL goes to sea, Bulletin of the American Meteorological Society, 100, 2285–2301, https://doi.org/https://doi.org/10.1175/BAMS-D-18-0233.1, 2019.

Schnitt, S., Foth, A., Kalesse-Los, H., Mech, M., Acquistapace, C., Jansen, F., Löhnert, U., Pospichal, B., Röttenbacher, J., Crewell, S., and Stevens, B.: Ground- and ship-based microwave radiometer measurements during EUREC ⁴ A, Earth System Science Data, 16, 681–700, https://doi.org/10.5194/essd-16-681-2024, 2024.

Schulz, H. and Stevens, B.: Observing the Tropical Atmosphere in Moisture Space, Journal of the Atmospheric Sciences, 75, 3313–3330, https://doi.org/10.1175/JAS-D-17-0375.1, 2018.

Schulz, H., Eastman, R., and Stevens, B.: Characterization and Evolution of Organized Shallow Convection in the Downstream North Atlantic Trades, Journal of Geophysical Research: Atmospheres, 126, https://doi.org/10.1029/2021JD034575, 2021.

https://doi.org/10.5194/egusphere-2026-4385
Preprint. Discussion started: 11 August 2026

Segura, H., Wing, A. A., Kalesse-Los, H., Carrasco, R., Ruppert Jr., J. H., Trosits, A., Nuijens, L., Ament, F., Blandfort, D., Bell, M. M., Bosser, P., Colón-Burgos, D., George, G., Habib, J., Horstmann, J., Jansen, F., Kluft, L., Kopte, R., Möller, K. O., Paschou, P., Schmidt, H., Schlundt, M., Serikov, I., Stelzner, M., Thompson, E. J., Wimmer, W., Dengler, M., and Klocke, D.: BOWTIE: ship-based measurements of atmosphere and ocean within the moist tropical Atlantic, Earth System Science Data, https://doi.org/10.5194/essd-2026-343, 2026.

Stevens, B., Farrell, D., Hirsch, L., Jansen, F., Nuijens, L., Serikov, I., Brügmann, B., Forde, M., Linne, H., Lonitz, K., and Prospero, J. M.: The Barbados Cloud Observatory: Anchoring Investigations of Clouds and Circulation on the Edge of the ITCZ, Bulletin of the American Meteorological Society, 97, 787–801, https://doi.org/10.1175/bams-d-14-00247.1, 2016.

Stevens, B., Bony, S., Farrell, D., Ament, F., Blyth, A., Fairall, C., Karstensen, J., Quinn, P. K., Speich, S., Acquistapace, C., Aemisegger, F., Albright, A. L., Bellenger, H., Bodenschatz, E., Caesar, K.-A., Chewitt-Lucas, R., de Boer, G., Delanoë, J., Denby, L., Ewald, F., Fildier, B., Forde, M., George, G., Gross, S., Hagen, M., Hausold, A., Heywood, K. J., Hirsch, L., Jacob, M., Jansen, F., Kinne, S., Klocke, D., Kölling, T., Konow, H., Lothon, M., Mohr, W., Naumann, A. K., Nuijens, L., Olivier, L., Pincus, R., Pöhlker, M., Reverdin, G., Roberts, G., Schnitt, S., Schulz, H., Siebesma, A. P., Stephan, C. C., Sullivan, P., Touzé-Peiffer, L., Vial, J., Vogel, R., Zuidema, P., Alexander, N., Alves, L., Arixi, S., Asmath, H., Bagheri, G., Baier, K., Bailey, A., Baranowski, D., Baron, A., Barrau, S., Barrett, P. A., Batier, F., Behrendt, A., Bendinger, A., Beucher, F., Bigorre, S., Blades, E., Blossey, P., Bock, O., Böing, S., Bosser, P., Bourras, D., Bouruet-Aubertot, P., Bower, K., Branellec, P., Branger, H., Brennek, M., Brewer, A., Brilouet, P.-E., Brügmann, B., Buehler, S. A., Burke, E., Burton, R., Calmer, R., Canonici, J.-C., Carton, X., Cato Jr., G., Charles, J. A., Chazette, P., Chen, Y., Chilinski, M. T., Choularton, T., Chuang, P., Clarke, S., Coe, H., Cornet, C., Coutris, P., Couvreux, F., Crewell, S., Cronin, T., Cui, Z., Cuypers, Y., Daley, A., Damerell, G. M., Dauhut, T., Deneke, H., Desbios, J.-P., Dörner, S., Donner, S., Douet, V., Drushka, K., Dütsch, M., Ehrlich, A., Emanuel, K., Emmanouilidis, A., Etienne, J.-C., Etienne-Leblanc, S., Faure, G., Feingold, G., Ferrero, L., Fix, A., Flamant, C., Flatau, P. J., Foltz, G. R., Forster, L., Furtuna, I., Gadian, A., Galewsky, J., Gallagher, M., Gallimore, P., Gaston, C., Gentemann, C., Geyskens, N., Giez, A., Gollop, J., Gouirand, I., Gourbeyre, C., de Graaf, D., de Groot, G. E., Grosz, R., Güttler, J., Gutleben, M., Hall, K., Harris, G., Helfer, K. C., Henze, D., Herbert, C., Holanda, B., Ibanez-Landeta, A., Intrieri, J., Iyer, S., Julien, F., Kalesse, H., Kazil, J., Kellman, A., Kidane, A. T., Kirchner, U., Klingebiel, M., Körner, M., Kremper, L. A., Kretzschmar, J., Krüger, O., Kumala, W., Kurz, A., L'Hégaret, P., Labaste, M., Lachlan-Cope, T., Laing, A., Landschützer, P., Lang, T., Lange, D., Lange, I., Laplace, C., Lavik, G., Laxenaire, R., Le Bihan, C., Leandro, M., Lefevre, N., Lena, M., Lenschow, D., Li, Q., Lloyd, G., Los, S., Losi, N., Lovell, O., Luneau, C., Makuch, P., Malinowski, S., Manta, G., Marinou, E., Marsden, N., Masson, S., Maury, N., Mayer, B., Mayers-Als, M., Mazel, C., McGeary, W., McWilliams, J. C., Mech, M., Mehlmann, M., Meroni, A. N., Mieslinger, T., Minikin, A., Minnett, P., Möller, G., Morfa Avalos, Y., Muller, C., Musat, I., Napoli, A., Neuberger, A., Noisel, C., Noone, D., Nordsiek, F., Nowak, J. L., Oswald, L., Parker, D. J., Peck, C., Person, R., Philippi, M., Plueddemann, A., Pöhlker, C., Pörtge, V., Pöschl, U., Pologne, L., Posyniak, M., Prange, M., Quiñones Meléndez, E., Radtke, J., Ramage, K., Reimann, J., Renault, L., Reus, K., Reyes, A., Ribbe, J., Ringel, M., Ritschel, M., Rocha, C. B., Rochetin, N., Röttenbacher, J., Rollo, C., Royer, H., Sadoulet, P., Saffin, L., Sandiford, S., Sandu, I., Schäfer, M., Schemann, V., Schirmacher, I., Schlenczek, O., Schmidt, J., Schröder, M., Schwarzenboeck, A., Sealy, A., Senff, C. J., Serikov, I., Shohan, S., Siddle, E., Smirnov, A., Späth, F., Spooner, B., Stolla, M. K., Szkółka, W., de Szoeke, S. P., Tarot, S., Tetoni, E., Thompson, E., Thomson, J., Tomassini, L., Totems, J., Ubele, A. A., Villiger, L., von Arx, J., Wagner, T., Walther, A., Webber, B., Wendisch, M., Whitehall, S., Wiltshire, A., Wing, A. A., Wirth, M., Wiskandt, J., Wolf, K., Worbes, L., Wright, E., Wulfmeyer, V., Young, S., Zhang, C., Zhang, D., Ziemen, F., Zinner, T., and Zöger, M.: EUREC ⁴ A, Earth System Science Data, 13, 4067–4119, https://doi.org/10.5194/essd-13-4067-2021, 2021.

Stevens, B., Bony, S., Gross, S., Klocke, D., Windmiller, J. M., Wing, A. A., von Bismarck, J., Brito, E., David, R. O., Delanoë, J., Farrell, D., and Wu, Y.: ORCESTRA: Organized Convection and EarthCARE Studies Over the Tropical Atlantic, Tellus, 79, 35–52, https://doi.org/10.16993/tellus.4123, 2026.

Tesche, M., Ansmann, A., Müller, D., Althausen, D., Mattis, I., Heese, B., Freudenthaler, V., Wiegner, M., Esselborn, M., Pisani, G., and Knippertz, P.: Vertical profiling of Saharan dust with Raman lidars and airborne HSRL in southern Morocco during SAMUM, Tellus B: Chemical and Physical Meteorology, 61, 144, https://doi.org/10.1111/j.1600-0889.2008.00390.x, 2009.

Tolentino, M., Bravo-Aranda, J. A., Guerrero-Rascado, J. L., Navas-Guzmán, F., Pérez-Ramírez, D., Alados-Arboledas, L., and Granados-Muñoz, M. J.: Long-term cloud characterization at the AGORA ACTRIS-CCRES station using a novel classification algorithm, Atmospheric Measurement Techniques, 19, 2079–2102, https://doi.org/10.5194/amt-19-2079-2026, 2026.

Tsamalis, C., Chédin, A., Pelon, J., and Capelle, V.: The seasonal vertical distribution of the Saharan Air Layer and its modulation by the wind, Atmospheric Chemistry and Physics, 13, 11 235–11 257, https://doi.org/https://doi.org/10.5194/acp-13-11235-2013, 2013.

Tukiainen, S., O'Connor, E., and Korpinen, A.: Cloudnetpy: A python package for processing cloud remote sensing data, Journal of Open Source Software, 5, 2123, https://doi.org/10.21105/joss.02123, 2020.

Tukiainen, S., Siipola, T., Leskinen, N., and O'Connor, E.: Remote sensing measurements during PaCE 2022 campaign, Earth System Science Data, 17, 3797–3806, https://doi.org/10.5194/essd-17-3797-2025, 2025.

Twohy, C. H., Kreidenweis, S. M., Eidhammer, T., Browell, E. V., Heymsfield, A. J., Bansemer, A. R., Anderson, B. E., Chen, G., Ismail, S., DeMott, P. J., and Van Den Heever, S. C.: Saharan dust particles nucleate droplets in eastern Atlantic clouds, Geophysical Research Letters, 36, https://doi.org/10.1029/2008GL035846, 2009.

Veselovskii, I., Goloub, P., Podvin, T., Bovchaliuk, V., Derimian, Y., Augustin, P., Fourmentin, M., Tanre, D., Korenskiy, M., Whiteman, D. N., Diallo, A., Ndiaye, T., Kolgotin, A., and Dubovik, O.: Retrieval of optical and physical properties of African dust from multiwavelength Raman lidar measurements during the SHADOW campaign in Senegal, Atmospheric Chemistry and Physics, 16, 7013–7028, https://doi.org/10.5194/acp-16-7013-2016, 2016.

Weinzierl, B., Ansmann, A., Prospero, J. M., Althausen, D., Benker, N., Chouza, F., Dollner, M., Farrell, D., Fomba, W. K., Freudenthaler, V., Gasteiger, J., Groß, S., Haarig, M., Heinold, B., Kandler, K., Kristensen, T. B., Mayol-Bracero, O. L., Müller, T., Reitebuch, O., Sauer, D., Schäfler, A., Schepanski, K., Spanu, A., Tegen, I., Toledano, C., and Walser, A.: The Saharan Aerosol Long-Range Transport and Aerosol–Cloud-Interaction Experiment: Overview and Selected Highlights, Bulletin of the American Meteorological Society, 98, 1427–1451, https://doi.org/10.1175/bams-d-15-00142.1, 2017.

Windmiller, J. M. and Stevens, B.: The inner life of the Atlantic Intertropical Convergence Zone, Quarterly Journal of the Royal Meteorological Society, 150, 523–543, https://doi.org/10.1002/qj.4610, 2024.

Winkler, M., Rixen, M., Beucher, F., Couvreux, F., Nam, C. C., Peyrillé, P., Schmidt, H., Segura, H., Wieners, K.-H., Alkilani-Brown, E., Coly, A. A., Biagioli, G., Bell, M. M., Brito, E., Chauvin, E., Capo, J., Colón-Burgos, D., Dawes, A., da Luz, J. C., Demiralay, Z., Douet, V., Ducastin, V., Dufaux, C., Dufresne, J.-L., Favot, F., Fiolleau, T., Fons, E., George, G., Gloeckner, H. M., Gonçalves, S., Gouttesoulard, L., Hayo, L., Hsiao, W.-T., Kennison, S., Kopelman, M., Lee, T.-Y., Le Gall, E., Lovato, M., Luschen, E., Maury, N., McKim, B., Netz, L., Ousseynou, D., Peters-von Gehlen, K., Pope, C., Poujol, B., Rivera Maldonado, N., Robbins-Blanch, N., Rochetin, N., Rowe, D., Romero Jure, P., Ruppert Jr., J. H., Segura Bermudez, J., Starr, J. C., Stelzner, M., Stoll, C., Syrett, M., Tekoe, A., Trules, J., Welty, C., Klocke, D., Vogel, R., Bony, S., Wing, A. A., and Stevens, B.: RAPSODI: radiosonde atmospheric profiles from ship and island platforms during ORCESTRA, collected to Decipher the ITCZ, Earth System Science Data, 18, 1833–1854, https://doi.org/10.5194/essd-18-1833-2026, 2026.

https://doi.org/10.5194/egusphere-2026-4385
Preprint. Discussion started: 11 August 2026

Wong, S. and Dessler, A. E.: Suppression of deep convection over the tropical North Atlantic by the Saharan Air Layer, Geophysical Research Letters, 32, https://doi.org/10.1029/2004GL022295, 2005.

Yang, W., Marshak, A., Kostinski, A. B., and Várnai, T.: Shape-induced gravitational sorting of Saharan dust during transatlantic voyage: Evidence from CALIOP lidar depolarization measurements, Geophysical Research Letters, 40, 3281–3286, https://doi.org/https://doi.org/10.1002/grl.50603, 2013.